**swiss*nuclear*: PEGASOS Refinement Project:
SP2 – Ground Motion Characterization**

Contract no. PMT-VT-1032

Seismic Shear Wave Velocity Determination and Hybrid Seismic Survey at the SED-Station AIGLE (Corbeyrier VD)

Date of Field Data Acquisition 7th April 2009

Revised Report

Client

swiss*nuclear*
Project PRP
Frohburgstrasse 17
4601 Olten

Contractor

GeoExpert ag
Seismic Prospecting
Ifangstrasse 12b
P.O. Box 451
8603 Schwerzenbach

8603 Schwerzenbach, 12th June 2009

INDEX

1   INTRODUCTION

1.1   Survey objectives

The seismic survey's main task is to provide information about the distribution function of the shear wave velocities in the depth interval of the uppermost 30 m along a 100 m long seismic profile.

Additionally, the following objectives are to be met:
- the mapping of the topography of the rock face, i.e. the thickness of the Quaternary deposits;
- the determination of the thickness of the weathered zone and its degree of decompaction at the bedrock surface;
- a general view of geological structures.

1.2   The choice of the appropriate surveying methods

Several methods are available for deriving the s-wave velocity distribution in the subsurface at any given position:
- in-situ measurement by down-hole or crosshole seismic surveying;
- shear-wave refraction tomography profiling;
- dispersion analysis of surface waves (MASW; **M**ultiple channel **A**nalysis of **S**urface **W**aves)

The surveys are to be carried out at, or as close as possible near some 20 SED earth quake monitoring stations in Switzerland. Ideally, the surveys are to be conducted on two orthogonal profiles in order to derive at their point of intersection a robust 1D s-wave velocity distribution function by correlation. To this end, the methods of MASW and shear-wave refraction tomography profiling are to be combined.

The results are to include the following fundamental parameters $v_{s,5}$, $v_{s,10}$, $v_{s,20}$, $v_{s,30}$, $v_{s,40}$, $v_{s,50}$, $v_{s,100}$ are to be calculated, also an error estimation of all values.

The data acquired for the MASW method are to be subjected to complementary **p-wave hybrid seismic data processing** in order to image the geological structures.

2 FIELD DATA ACQUISITION PARTICULARS

2.1 Time Schedule

Date	Time	Activities / remarks
07.04.2009	0730	arrival from Torny-le-Grand FR
	0730 - 0830	lay-out of recording spread profile 1 p- and p-wave
	0840 - 0910	compressional wave data recording profile 1
	0915 - 1000	shear wave data recording profile 1
	1000 - 1030	retrieval of the recording spread
	1115 - 1200	lay-out of recording spread profile 2 s- and p-wave
	1330 - 1400	compressional wave data recording profile 2
	1400 - 1430	shear wave data recording profile 2
	1430 - 1500	retrieval of the recording spread
	1500	departure from site

2.2 Summary of Data Acquisition Parameters

Compressional Wave Data Acquisition

# of active channels	96
geophone type	4.5 Hz natural frequency, vertical velocimeter
receiver station spacing	1.0 m
# of geophones/station	1
source point spacing	2.0 m
source type	vertical hammer (6 kg) striking on a horizontal metal plate
sampling rate	500 µs
recording time	2048 ms
field filters	0.5 Hz LC, anti-alias
# of field records	60 (line 09SN_02AIGLE-P1) and 61 (line 09SN_02AIGLE-P2)

Shear Wave Data Acquisition

# of active channels	48
geophone type	10 Hz natural frequency, horizontal velocimeter
receiver station spacing	2.0 m
# of geophones/station	1
source point spacing	4.0 m
source type	horizontal hammer (6 kg) striking horizontally at a metal-plated wooden beam anchored to the ground by means of 20 cm long spikes
sampling rate	500 µs
recording time	512 ms
field filters	2 Hz LC, anti-alias
# of field records	52 @ 26 positions (line 09SN_02AIGLE-S1) and 50 @ 25 positions (line 2)

Fig. 2.1:   S-wave data acquisition at profile 09SN_02AIGLE-S1. In front: motorized barrow with shear wave source. In red the 4.5 Hz vertical receivers and in yellow the 10 Hz horizontal receiver. In background: portal into the military bunker.

2.3 Composition of Seismic Field Crew

Personnel
Philippe Corboz   Dipl. Natw. ETHZ, geophysicist , party chief
Dieter Martin   Dipl.-Geolog, University of Freiburg I. Br., operator
Kieron Lynch   assistant, spread lay-out and activation of seismic source

Equipment
96   vertical geophones 4.5 Hz
48   horizontal geophones 10 Hz
6   seismic cables
1   seismic acquisition system Summit Compact, 96 channels
1   laptop computer for data acquisition
3   walkie-talkies
1   hammer 6 kg
1   steel plate
1   metal-plated wooden beam
1   motorized barrow
1   van (FIAT Ducato 4x4)

2.4 Location

The seismic monitoring station AIGLE (Corbeyrier VD) is situated in military bunker on the flank of a Jurassic sediment ridge in western, canton of Vaud. The monitoring station is positioned on Malm limestones, a hard and seismic fast rock. The lines of the seismic survey described here are placed partly on loose talus covering the flanks, line 09SN_02AIGLE-1 possibly also Triasic sediments.

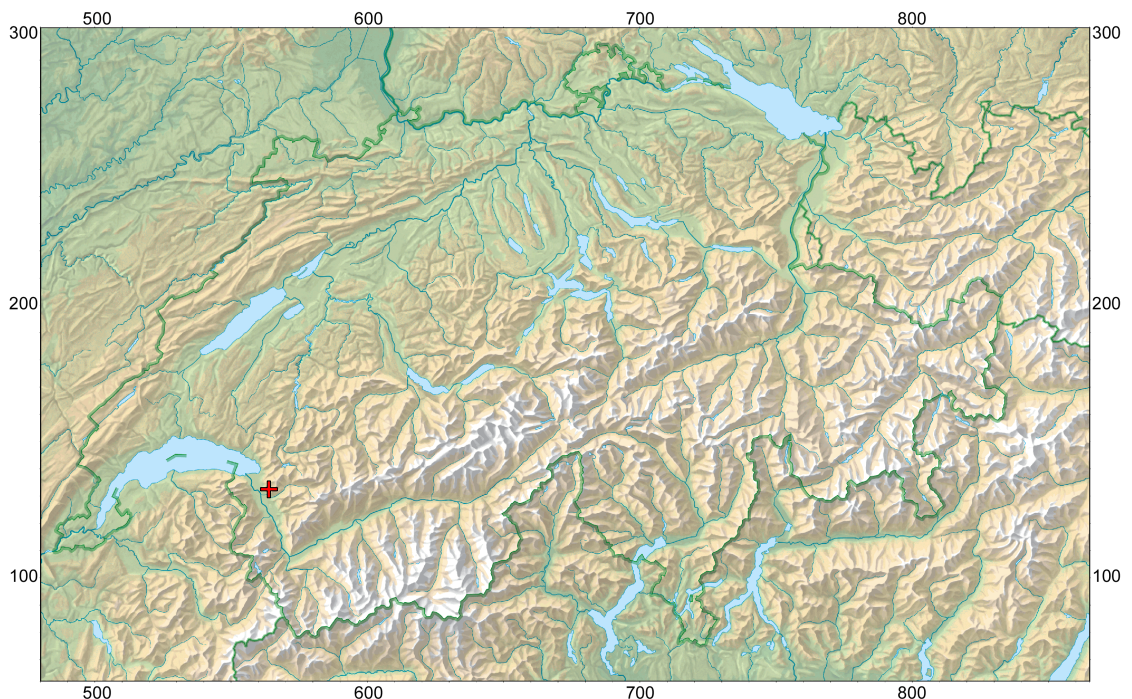Fig. 2.2:   The red cross marked seismic monitoring station AIGLE (Corbeyrier VD) is located in Jurassic sediments (Malm). (map: geodata @ swisstopo).

2.5 Recording Conditions and Line Setup

The measurements at AIGLE could be done in dry and warm conditions. Building works for the bunker during the recordings partly disturbed the data considerably.

In general, the seismic data quality obtained at AIGLE is to be rated as fair.

Legend

⊕ SED station

~ seismic line

0 10 20 30 40 50m

equidistance: 10 m

09SN_02AIGLE-1

01

562 700

132 300

96

09SN_02AIGLE-2

01

96

Coordinates Line 09SN_02AIGLE-1:
Station 01: 562.664 / 132.335
Station 96: 562.736 / 132.295
approx. SED station offset from 01: 26 m WNW

Coordinates Line 09SN_02AIGLE-2:
Station 01: 562.642 / 132.339
Station 96: 562.599 / 132.235
approx. SED station offset from 01: 23 m N
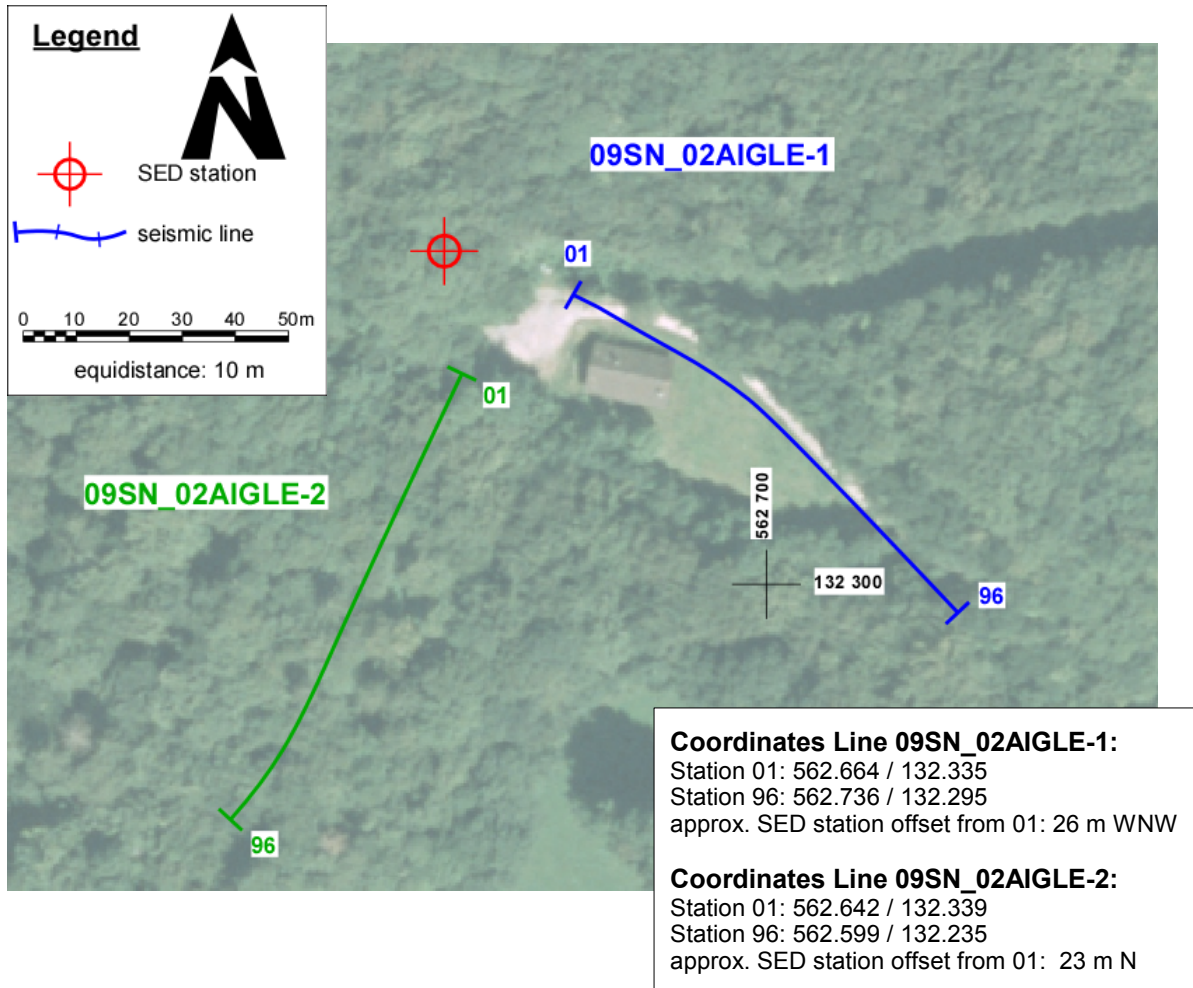
Fig. 2.3:   Situation map with the trace of seismic profile 09SN_02AIGLE-1 and -2.
              (background map: © Etat de Vaud, swisstopo)

3 SEISMIC DATA PROCESSING AND IMAGING OF THE RESULTS

3.1 General Remarks

- For the shear and compressional wave refraction seismic evaluation the package **RAYFRACT** by Intelligent Resources Ltd., Vancouver CAN, was used. The system features the technique of diving wave tomography (www.rayfract.com).

- The system **SPW** (**S**eismic **P**rocessing **W**orkshop) of Parallel Geoscience Corporation, Austin US-TX, was used for reflection seismic data processing (www.parallelgeo.com).

- Data processing of surface waves (MASW processing) was conducted with the software package **SurfSeis** V2.0 of Kansas Geological Survey in Lawrence US-KS.

A detailed description of the various surveying methods will be included in the general summary report.

3.2 Shear Wave Refraction Tomography

3.2.1 Reformatting and field geometry assignment

After reformatting the field data into the Rayfract format the field geometry is applied.

3.2.2 First break time picking

At each shot position, two seismic records were acquired in both activation directions. These two records are displayed superimposed with different colors on each other in Fig 3.2a together with the manually determined first arrival time picks.
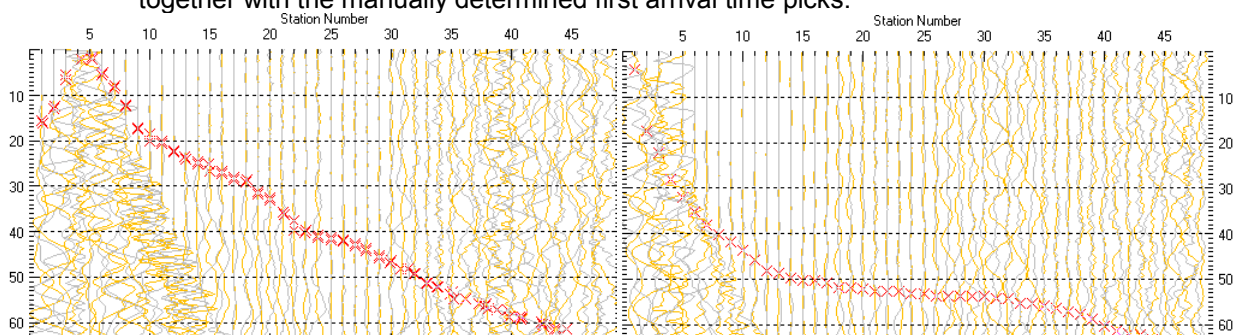

Fig. 3.2a: High quality dual field record of line 09SN_02AIGLE-S1 (left) and 09SN_02AIGLE-S2 (right).showing at each station the s-wave traces with opposing polarities in different colors. The manually picked s-wave refraction arrivals at each station are marked with an **x**. The station spacing is 2 m, profile station number 00 = profile meter 0; profile station number 48 = profile meter 96.
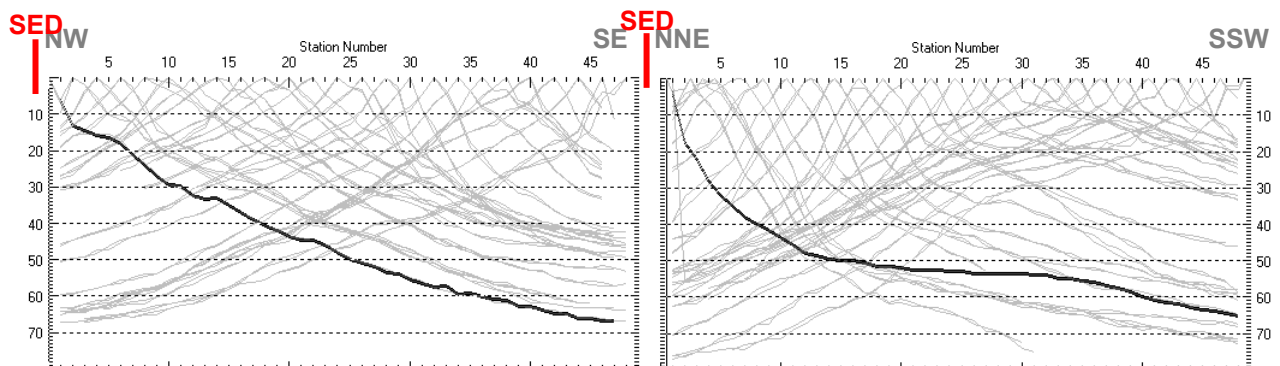

Fig. 3.2b: Curves of s-wave first break time picks of line 09SN_02AIGLE-S1 (left) and -S2 (right).

3.2.3 Analytical Determination of Refraction Velocities

An initial 1D-velocity function (averaged 1D velocity-depth profiles derived by the Delta-t-V method, see Tab. 3.2a) is determined in the 3-dimensional time-offset-CMP-domain of all first break arrival time curves in the 3-dimensional time-offset-CMP-domain (see. Fig. 3.2c).

Depth [m]	Vs [m/s]	Depth [m]	Vs [m/s]
0.0	507	0.0	717
0.4	550	0.3	737
0.7	552	0.7	776
1.1	523	1.0	824
1.4	555	1.4	866
2.1	591	2.1	945
2.8	696	2.8	1027
3.9	875	3.8	1131
5.3	1121	5.2	1235
6.9	1335	6.8	1338
9.2	1459	9.1	1509
12.3	1588	12.1	1695
16.0	1788	15.7	1803
20.9	2000	20.6	2050
27.3	2423	26.9	2396
35.9	2564	35.3	3178
46.7	4672		

Tab. 3.2a: Initial 1D s-wave velocity function derived from real data of line 09SN_02AIGLE-S1 (mean values between profile meters 65 and 75) and of line 09SN_02AIGLE-S2 (mean values between profile meters 55 and 75).
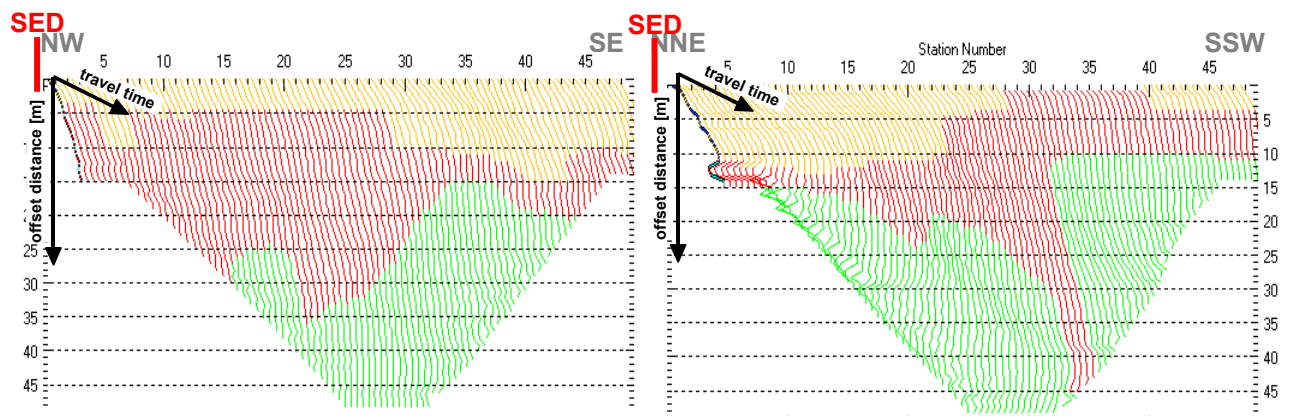

Fig. 3.2c: 3-dimensional distance-travel time diagrams of line 09SN_02AIGLE-S1 (left) and -S2 (right) at the mid-points between source points and receiver stations are instrumental when using the analytical CMP derivation of the initial velocity field.
The horizontal axes are the along the CMP positions and the travel time respectively, the vertical axis denotes the offset distance between source and receiver positions. The colors represent different velocity layers. The station spacing is 2 m, profile station number 00 = profile meter 0; profile station number 48 = profile meter 96. The colors represent different velocity layers.

3.2.4 Tomographic inversion of the velocity gradient field by iterative modeling

The velocity field is iteratively refined by the subsequent Wavepath Eikonal Traveltime (WET) tomographic inversion process. The inversion results are portrayed in Fig. 3.2d as a gridded velocity contour section and in Fig. 3.2e as a ray path density section.
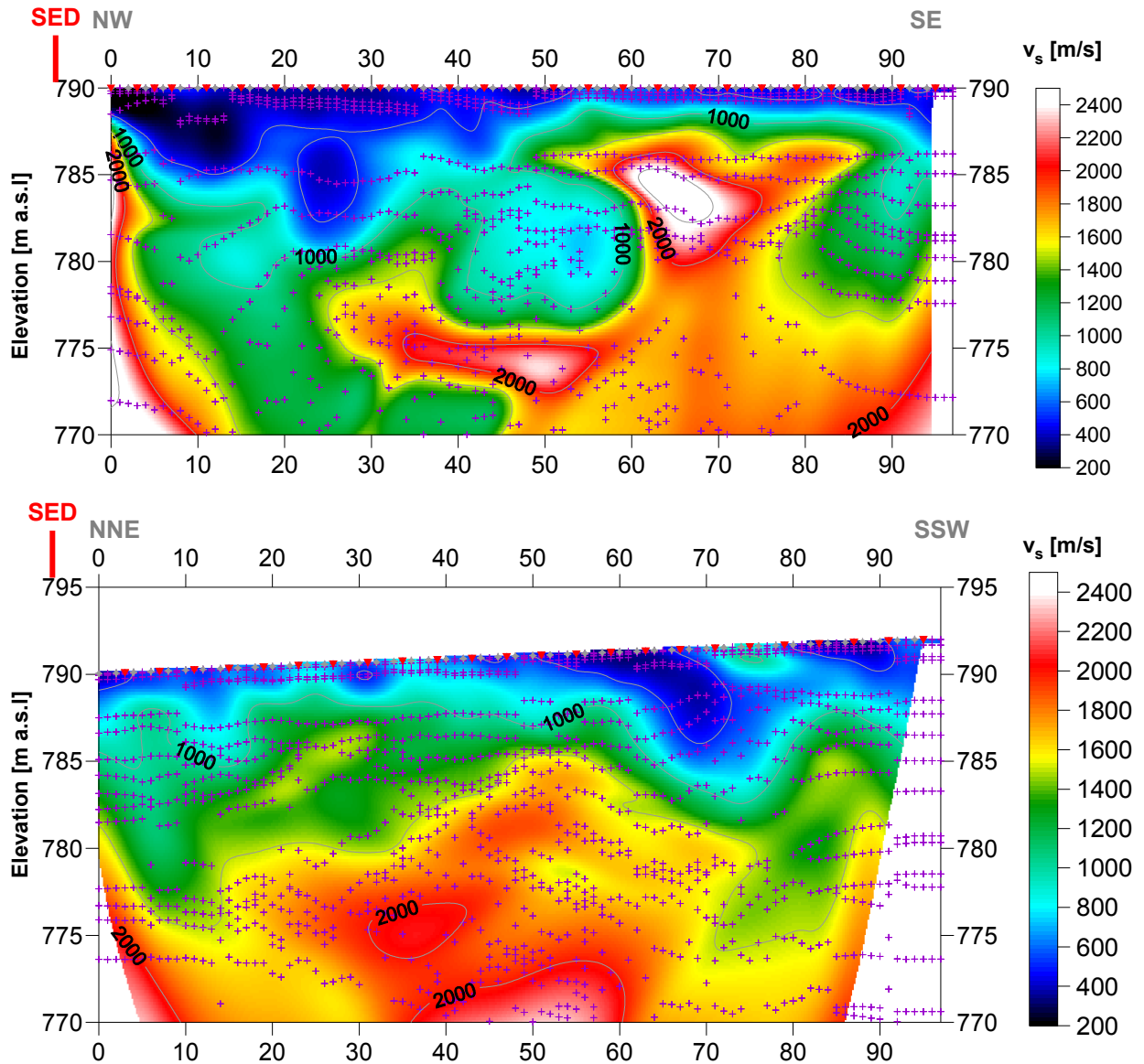

Fig. 3.2d: *Shear wave velocity field of the line 09SN_02AIGLE-S1 (top) and -S2. (bottom). Red/white colors denote solid rock, blue/black colors point to unconsolidated sediments and soil. Vertical axis: elevation [m a.s.l]; horizontal axis: profile meter; color encoded scale: vs [m/s]; vertical exaggeration: 2:1; gray diamonds: receiver positions; red triangles: source positions; magenta crosses: positions of determined velocity values. The station spacing is 2 m, profile meter 0 = profile station number 00, profile meter 96 = profile station number 48.*
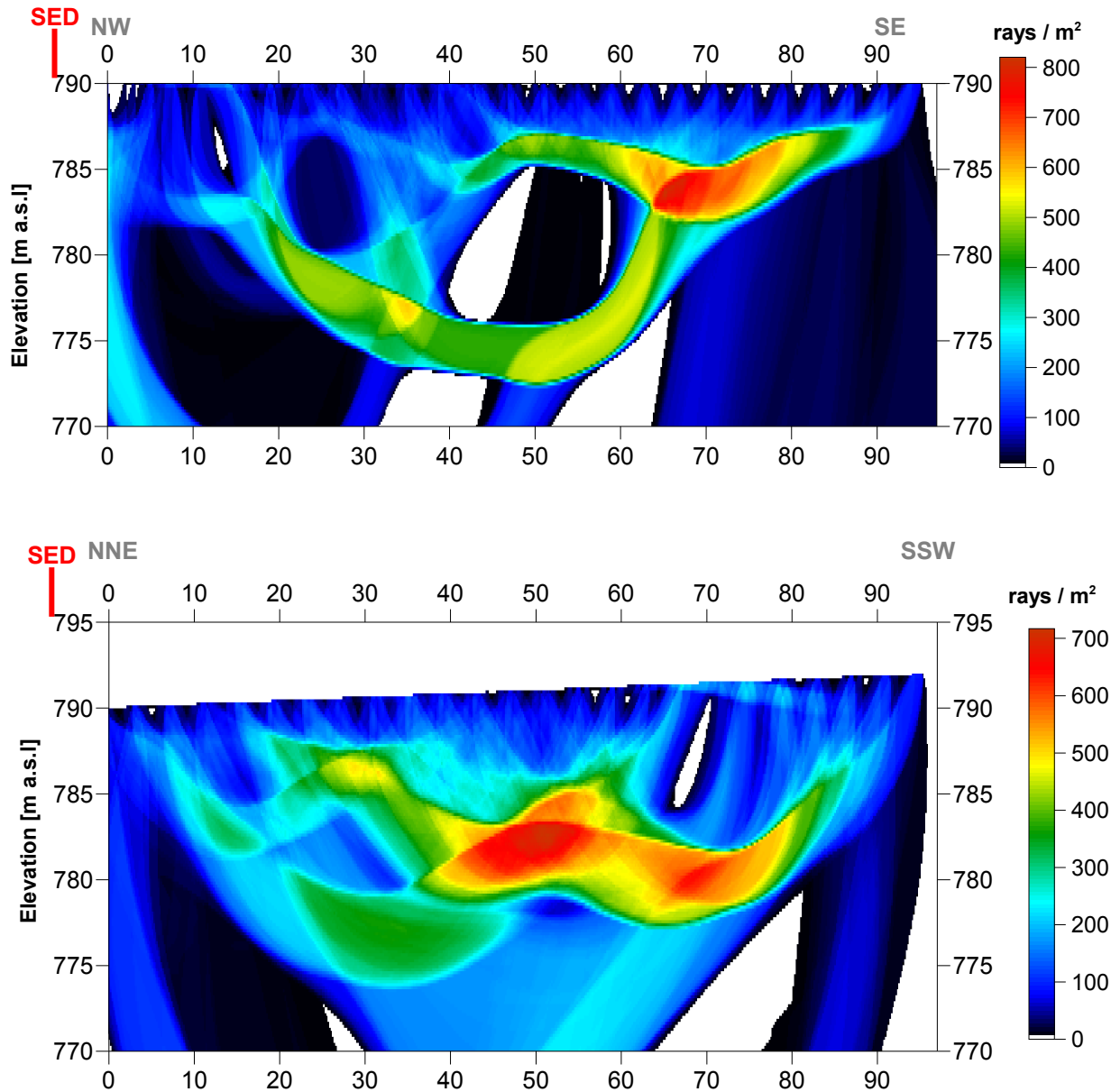
Fig. 3.2e: *Shear wave ray path density along the seismic line 09SN_02AIGLE-S1 (top) and -S2 (bottom). Red/white colors indicate high velocity contrasts (usually at the bedrock surface), blue/black colors denote low coverage areas. Vertical axis: elevation [m a.s.l]; horizontal axis: profile meter; color encoded scale: ray paths per m²; vertical exaggeration: 2:1. The station spacing is 2 m, profile meter 0 = profile station 00, profile meter 96 = profile station 48.*

Depth [m]	Vs [m/s]
0.0	485
3.2	1616
6.4	2434
9.6	1931
12.8	1731
16.0	1779
19.0	1833
22.2	1998
25.4	2200
28.6	2362
31.8	2534
34.8	2810
38.0	3082
41.2	3331
44.4	3660
47.6	4039
50.6	4334
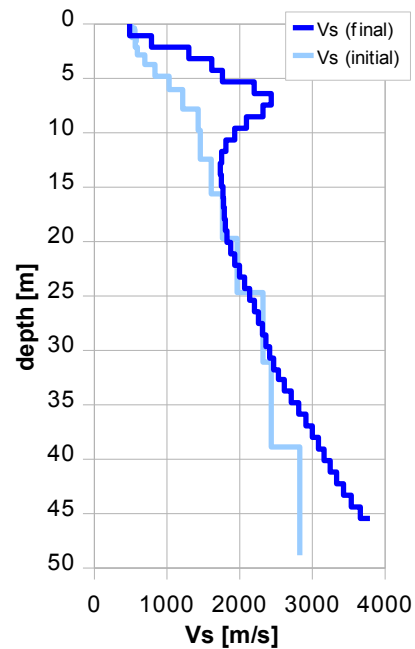
Tab. 3.2b: Final 1D s-wave velocity model derived from real data of line 09SN_02AIGLE-S1 (horizontal average of all values) for the profile segment (between profile meters 65 and 75) with a geological setting resembling the one at the SED station. The calculated values of the initial 1D s-wave velocity model are given in Tab. 3.2a.

Depth [m]	Vs [m/s]
0.0	472
2.1	685
4.2	880
6.3	1241
8.4	1493
10.5	1642
12.6	1599
14.7	1689
16.6	1765
18.7	1827
20.8	1880
22.9	1950
25.0	2058
27.1	2178
29.2	2302
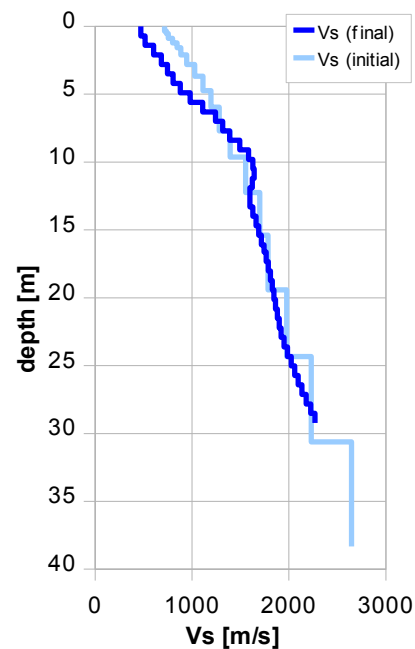
Tab. 3.2c: Final 1D s-wave velocity model derived from real data of line 09SN_02AIGLE-S2 (horizontal average of all values) for the profile segment (between profile meters 55 and 75) with a geological setting resembling the one at the SED station. The calculated values of the initial 1D s-wave velocity model are given in Tab. 3.2a.

3.3 MASW Processing

3.3.1 Reformatting and field geometry assignment

The data preparation steps for the dispersion analysis include
- the assignment of the field acquisition geometry
- the selection of suitable offset ranges (=arrays) between 10 m and 50 m for dispersion, and the splitting of the field records in forward and reverse shooting direction data sets
- the reformatting of the data into the specific KGS format

X - - ... - - o-o-o-...-o-o-o (forward shooting or so-called PLUS direction)
respectively
    o-o-o-...-o-o-o - - ... - - X (reverse shooting or so-called MINUS direction).

where   **X** = shot position
           o = receiver station
           - = 1.0 m offset

The active array used at SED-station AIGLE are the receiver station in the shot offset range between 10 and 50 m.

3.3.2 Calculating the dispersion image (overtone)

The result of dispersion analysis is the color encoded acoustic energy distribution in the phase velocity - frequency plane (see Fig. 3.3a and b).
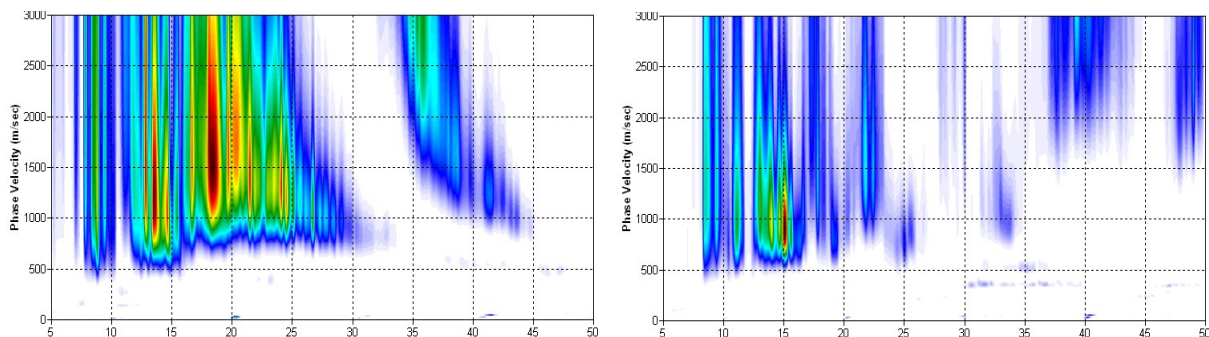

Fig. 3.3a: Dispersion image of fair quality data (left) of midpoint station 60 as found on 60 % and of deficient quality data (right) of midpoint station 54 representing about 40 % of the MASW dataset of site AIGLE.
Horizontal axis: frequency from 5 to 50 Hz; vertical axis: phase velocity from 0 to 2000 m/s; color code: colors from white (no energy) to blue - green - yellow - red - black point to increasing energy amplitude values.

3.3.3 Analysis of the dispersion image

In the dispersion graphs as calculated in section 3.3.2 above, the curves joining the amplitude peaks of the fundamental modes are determined either by subjective inspection or in a semi-automated manner. On datasets with poorly defined amplitude peaks or with a highly irregular alignment of the peaks, the danger of obtaining improbable or wrong results is real and can only be mitigated by the processing experience and the a-priori knowledge of the geological setting by the geophysicist responsible for the data evaluation.
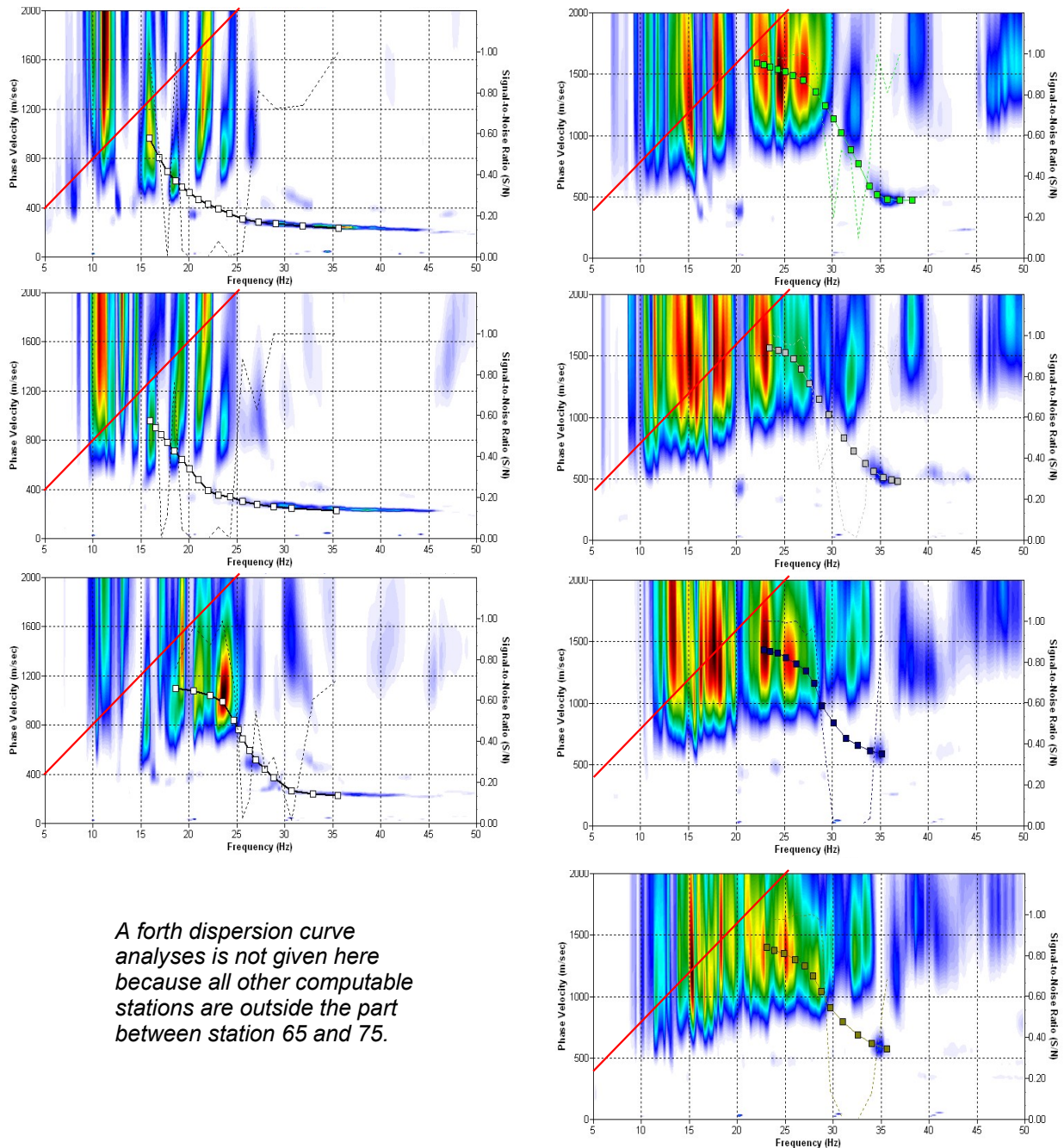
A forth dispersion curve analyses is not given here because all other computable stations are outside the part between station 65 and 75.

Fig. 3.3b: The manually picked dispersion images used for the derivation of the shear wave velocity section on line 09SN_02AIGLE-M1. The dispersion curves (squares) are determined by link-ing the peaks of high energy. Note that 'higher modes' may at times produce higher energy peaks than the fundamental mode required for the analysis.
dotted fine line: signal-noise ratio for the designated f-v_{ph} – value.
red line: high resolution beam-forming curve for v_{max}.
1st row: left: station 65 @ PLUS direction; right: station 67 @ MINUS direction
2nd row: left: station 67 @ PLUS direction; right: station 69 @ MINUS direction
3rd row: left: station 75 @ PLUS direction; right: station 73 @ MINUS direction
4th row: n/a   right: station 75 @ MINUS direction
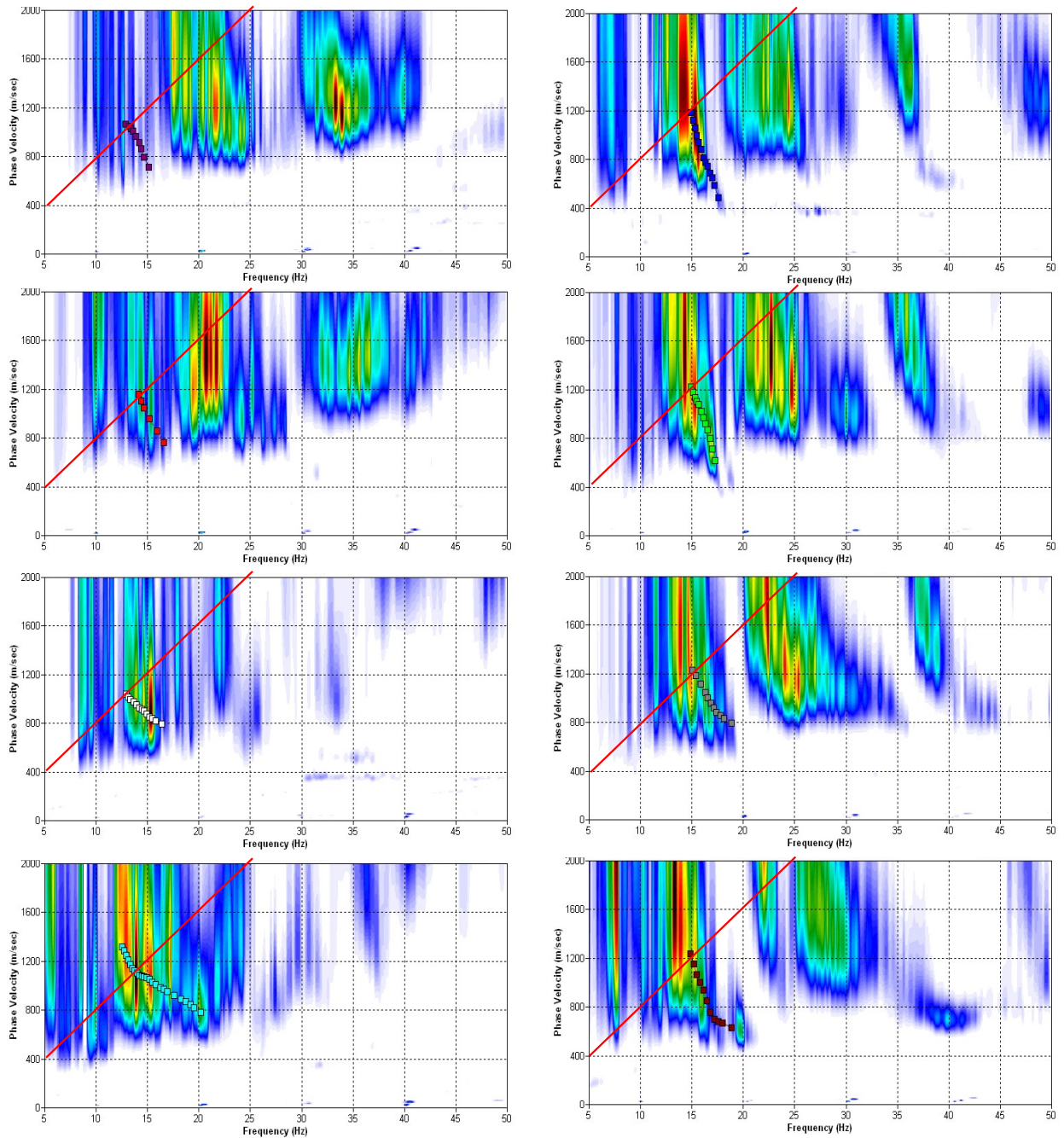
Fig. 3.3c: The manually picked dispersion images used for the derivation of the shear wave velocity section on line 09SN_02AIGLE-M2. The dispersion curves (squares) are determined by linking the peaks of high energy. Note that 'higher modes' may at times produce higher energy peaks than the fundamental mode required for the analysis.
dotted fine line: signal-noise ratio for the designated f-v_{ph} – value.
red line: high resolution beam-forming curve for v_{max}.
1st row: left: station 55 @ PLUS direction; right: station 58 @ MINUS direction
2nd row: left: station 59 @ PLUS direction; right: station 60 @ MINUS direction
3rd row: left: station 67 @ PLUS direction; right: station 66 @ MINUS direction
4th row: left: station 71 @ PLUS direction; right: station 72 @ MINUS direction

3.3.4   Inversion of dispersion curves resulting in a 1D shear wave velocity distribution

Inversion of the extracted dispersion curves was performed using the algorithm described by Xia et al. (1999).

The inversion process is started by setting the maximum depth (z_{max}) to be in the order of 30% of the largest wavelength for an initial model consisting of 10 layers of increasing thicknesses. For all 10 layers the Poisson's ratio is assumed to be 0.4 and the rock/soil density to be 2.0 g/cm^3. The inversion process is concluded either after twelve iterations or when the convergence condition of a RMS-error of less than 3 m/s (phase velocity) is met.
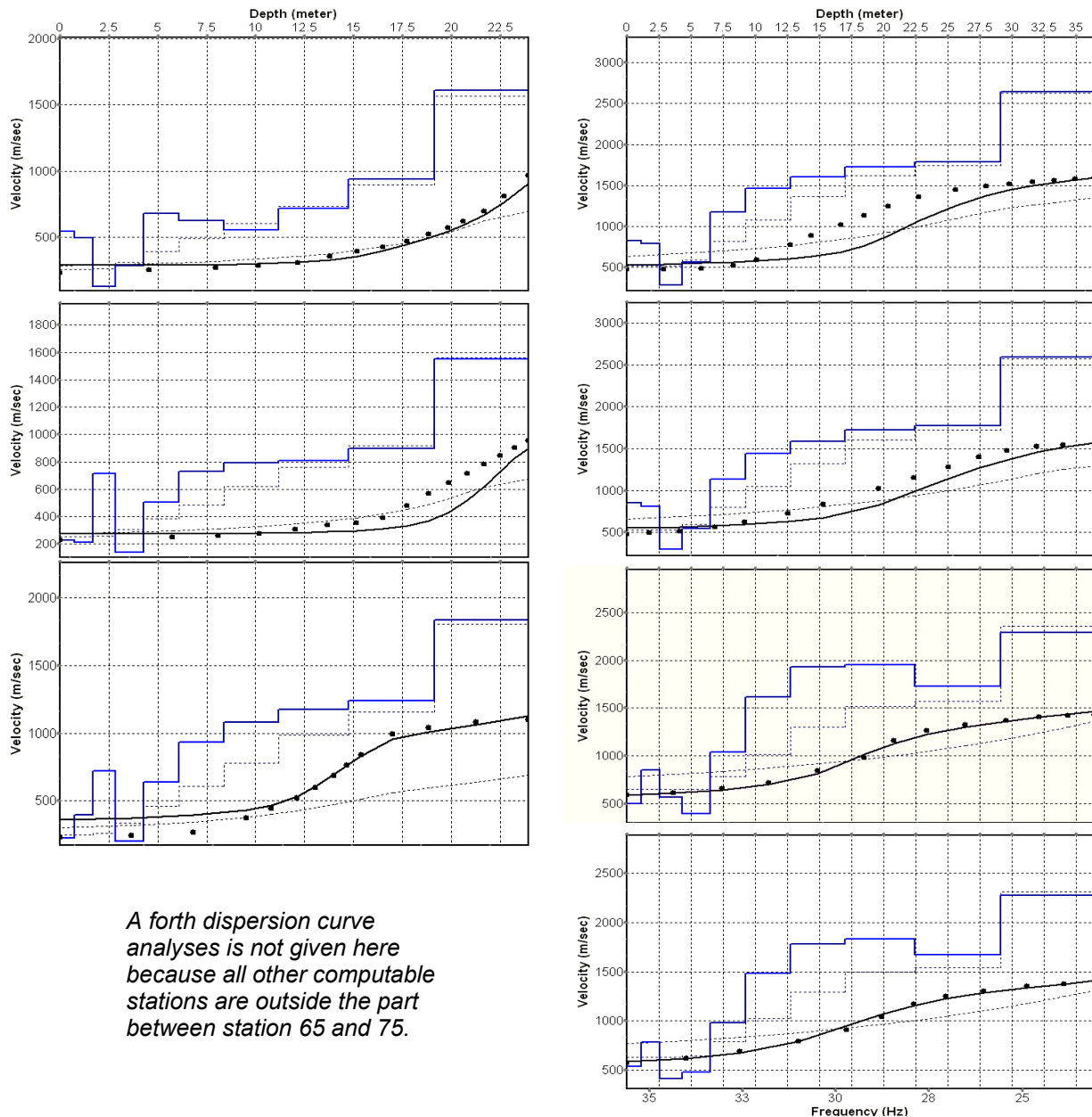
A forth dispersion curve analyses is not given here because all other computable stations are outside the part between station 65 and 75.

Fig. 3.3d: *Inversion results of dispersion curves of dataset at line 09SN_02AIGLE-M1.*
brown: Inversion of dispersion curve (dots) resp. of the modeled dispersion curve (dotted line: initial model; continuous line: end model). Horizontal axis: frequency Hz, vertical axis: v$_s$.
blue: 10-layer-model (dotted: initial model, continuous line: final model). Horizontal axis: depth, vertical axis: phase velocity resp. v$_s$).
1st row: left: station 65 @ PLUS direction; right: station 67 @ MINUS direction
2nd row: left: station 67 @ PLUS direction; right: station 69 @ MINUS direction
3rd row: left: station 75 @ PLUS direction; right: station 73 @ MINUS direction
4th row: n/a   right: station 75 @ MINUS direction
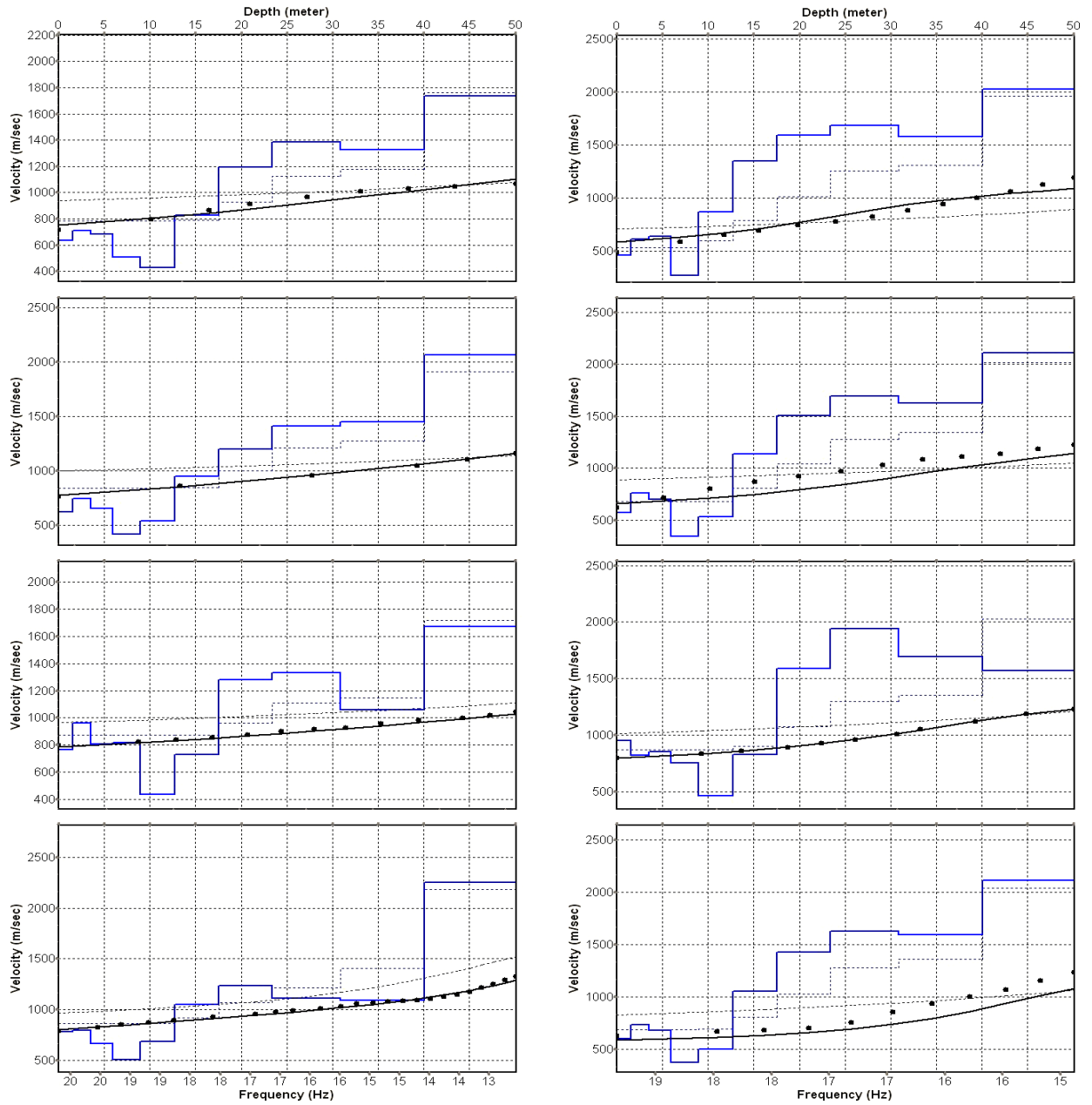
Fig. 3.3e: Inversion results of dispersion curves of dataset at line 09SN_02AIGLE-M2.
__brown__: Inversion of dispersion curve (dots) resp. of the modeled dispersion curve (dotted
line: initial model; continuous line: end model). Horizontal axis: frequency Hz, vertical axis: v_s.
__blue__: 10-layer-model (dotted: initial model, continuous line: final model). Horizontal axis:
depth, vertical axis: phase velocity resp. v_s).
1st row: left: station 55 @ PLUS direction; right: station 58 @ MINUS direction
2nd row: left: station 59 @ PLUS direction; right: station 60 @ MINUS direction
3rd row: left: station 67 @ PLUS direction; right: station 66 @ MINUS direction
4th row: left: station 71 @ PLUS direction; right: station 72 @ MINUS direction

Dispersion analyses of records with longer receiver arrays should – by theory – increase the investigation depth. At AIGLE, with both lines and both directions, MASW processing with the maximal array length of 96 m improves the results (Fig. 3.3f and 3.3g).
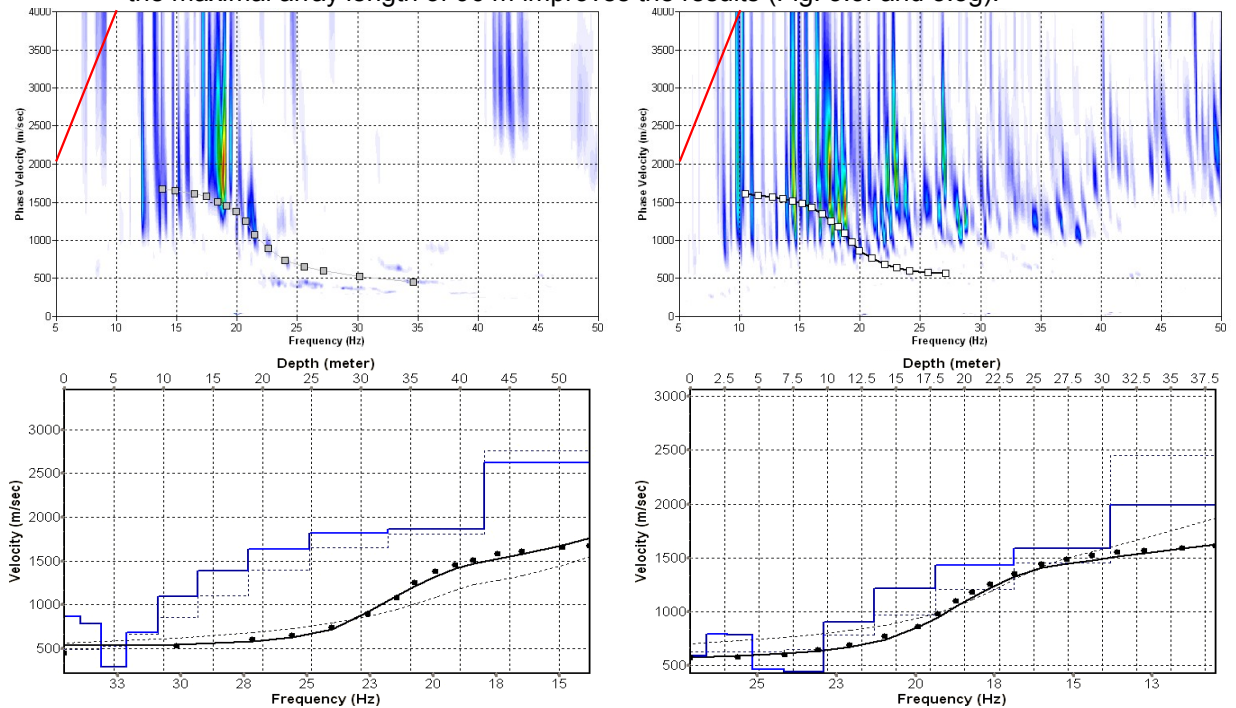

Fig. 3.3f: Top: dispersion images of over-all arrays (10...116 m offset) of line 09SN_02AIGLE-M1 in PLUS (left) and MINUS (right) direction. Red line: high resolution beam-forming curve for v*max*.
Below: The two respective inversion results; **brown**: inversion of dispersion curve; **blue**: 10-layer-model. Horizontal axis: depth, vertical axis: phase velocity resp. v*s*.
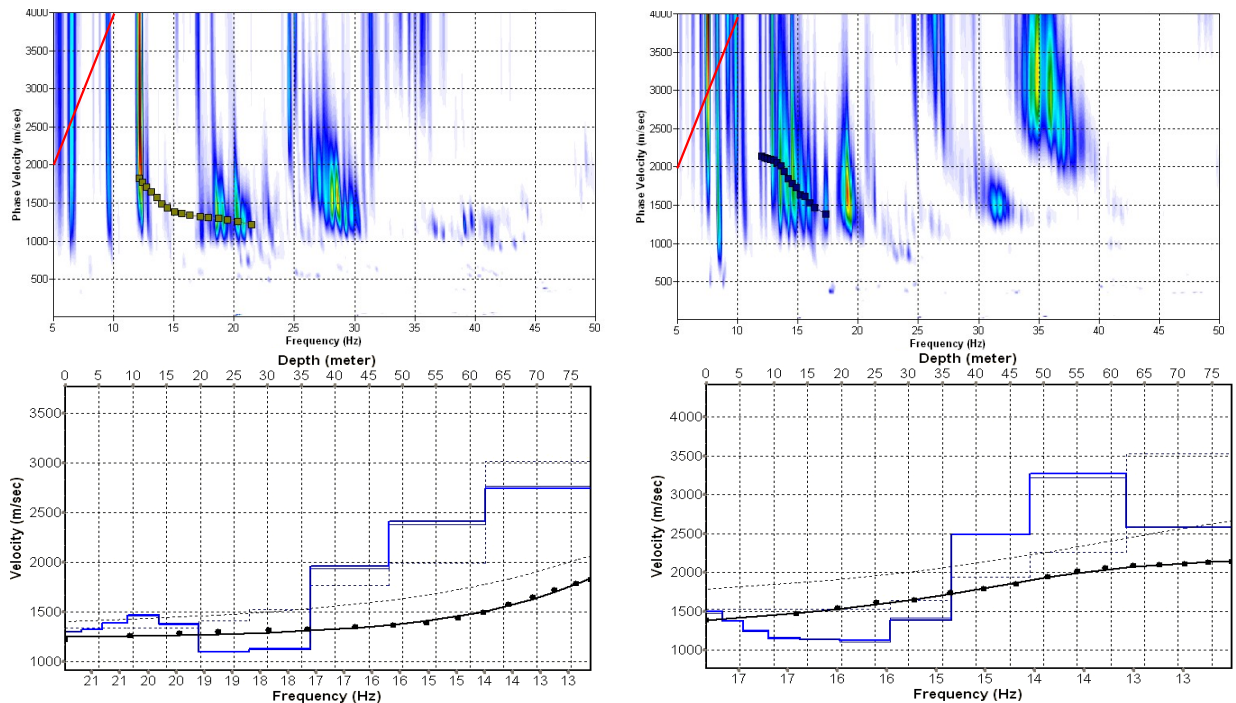

Fig. 3.3g: Top: dispersion images of over-all arrays (10...106 m offset) of line 09SN_02AIGLE-M2 in PLUS (left) and MINUS (right) direction. Red line: high resolution beam-forming curve for v*max*.
Below: The two respective inversion results; **brown**: inversion of dispersion curve; **blue**: 10-layer-model. Horizontal axis: depth, vertical axis: phase velocity resp. v*s*.

3.3.5 Gridding and plotting of 2D v$_s$-velocity field

By assembling the 1D v$_s$ - depth functions of all stations the final 2D v$_s$-field is derived using a Kriging gridding procedure as portrayed in Fig. 3.3h and 3.3i below:
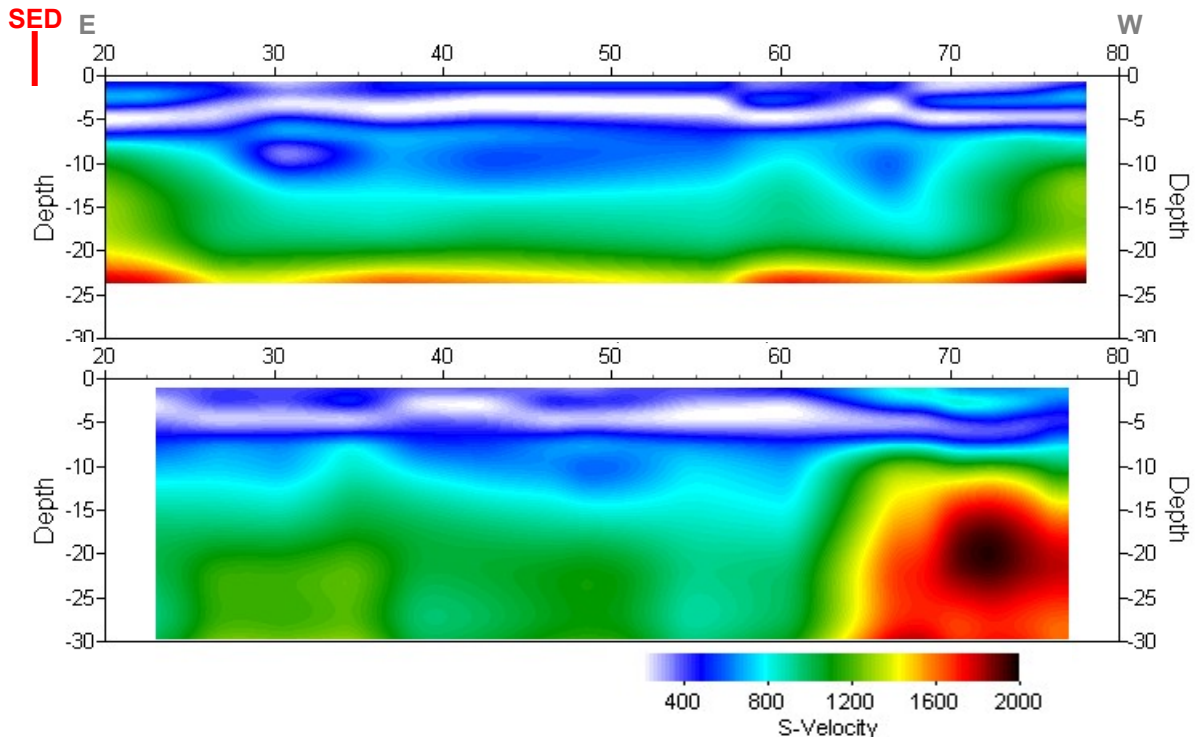

Fig. 3.3h: PLUS- (above) and MINUS- (below)-MASW-processed shear wave velocity fields of line 09SN_02AIGLE-M1. Profile station spacing is 1 m.
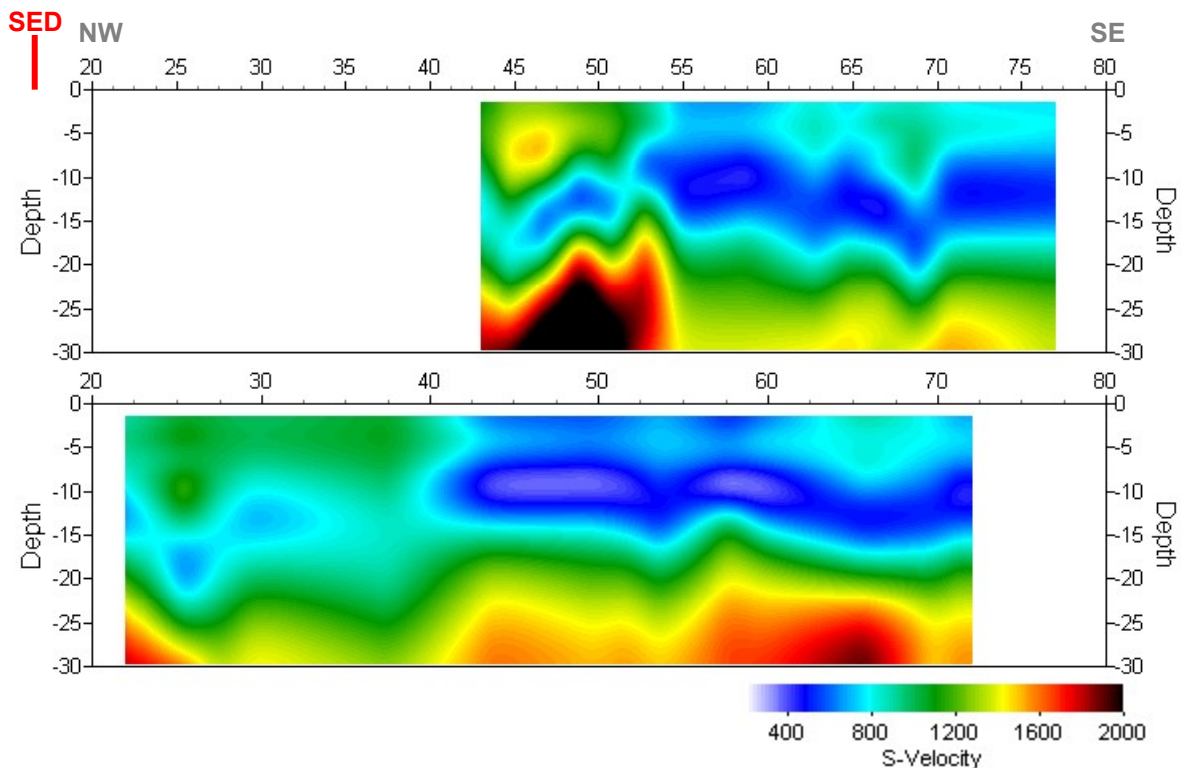

Fig. 3.3i: PLUS- (above) and MINUS- (below)-MASW-processed shear wave velocity fields of line 09SN_02AIGLE-M2. Profile station spacing is 1 m.

3.3.6 Calculation of the average shear wave velocity

In order to calculate a representative shear wave velocity-depth function of line 09SN_02AIGLE-M1 at the SED station, all computed 1D-v_s-depth functions between seismic profile station no. 65 and 75 – that are four profiles in each direction – are averaged (non-weighted mean values). The v_s-depth-function is shown in Tab. 3.3a.

Depth [m]	Vs+ [m/s]	Vs- [m/s]	Vs [m/s]
0.0	464	467	466
2.1	447	708	577
3.6	438	448	443
5.4	677	275	476
7.7	860	736	798
10.5	1082	1053	1067
14.1	1285	1304	1295
18.6	1355	1362	1358
24.2	1451	1608	1530
30.2	1745	2052	1899
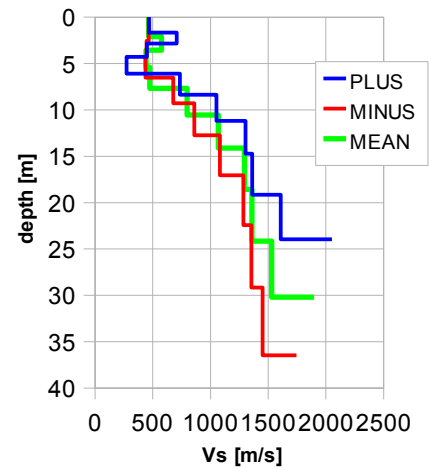
Tab. 3.3a: Averaged vs - depth function of line 09SN_02AIGLE-M1 at the SED station AIGLE.
Blue line: MASW-'PLUS' processing, red line: MASW-'MINUS' processing;
green line: average of PLUS- and MINUS-functions.

In order to calculate an representative shear wave velocity-depth function of line 09SN_02AIGLE-M2 at the SED station, all computed 1D-v_s-depth functions between seismic profile station no. 55 and 75 are averaged (non-weighted mean values). The resulting v_s-depth-function is shown in Tab. 3.3b.

Depth [m]	Vs- [m/s]	Vs+ [m/s]	Vs [m/s]
0.0	758	915	837
3.5	808	925	866
5.9	701	802	752
9.0	487	627	557
12.8	758	754	756
17.5	1293	1174	1233
23.4	1642	1507	1575
30.8	1774	1581	1677
40.1	2091	1800	1946
50.1	2114	1750	1932
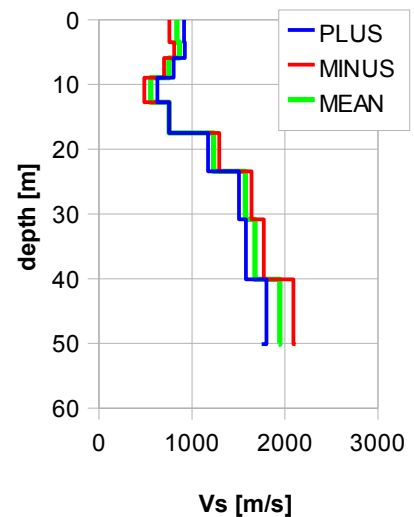
Tab. 3.3b: Averaged v_s - depth function of line 09SN_02AIGLE-M2 at the SED station AIGLE.
Blue line: MASW-'PLUS' processing, red line: MASW-'MINUS' processing;
green line: average of PLUS- and MINUS-functions.

The inversion of the four 100 m-array dispersion curves data (10 to 106 m offset, see Fig. 3.3f and 3.3g) are given in Tab. 3.3c. These values are complemented with the values derived of the 40 m-arrays analyses (Tab. 3.3a and 3.3b).

	100 m array							40 m array					
depth	m1+	m1-	m2+	m2-	m1	m2	m	depth	m1	depth	m2	depth	m
1.9	869	594	1300	1498	732	1336	921	0.0	466	0.0	837	0.0	651
4.3	785	790	1321	1371	788	1279	966	2.1	577	3.5	866	2.8	722
7.3	289	786	1390	1237	538	1265	822	3.6	443	5.9	752	4.7	597
11.1	683	463	1464	1151	573	1294	870	5.4	476	9.0	557	7.2	516
15.7	1098	442	1378	1140	770	1383	973	7.7	798	12.8	756	10.2	777
21.6	1385	904	1096	1123	1145	2184	1129	10.5	1067	17.5	1233	14.0	1150
28.9	1632	1218	1123	1387	1425	1851	1325	14.1	1295	23.4	1575	18.8	1435
38.0	1816	1431	1961	2487	1623	1961	1736	18.6	1358	30.8	1677	24.7	1518
49.5	1867	1586	2410	3271	1726	2410	1954	24.2	1530	40.1	1946	32.1	1738
61.8	2624	1992	2742	2579	2308	2742	2453	30.2	1899	50.1	1932	40.2	1915

Tab. 3.3c: v_s-depth values of the four MASW-derived dispersion curves of both seismic line 09SN_02AIGLE-M1 and 09SN_02AIGLE-M2 using 100 m-arrays. The dispersion curves are shown in Fig. 3.3f and Fig 3.3g.

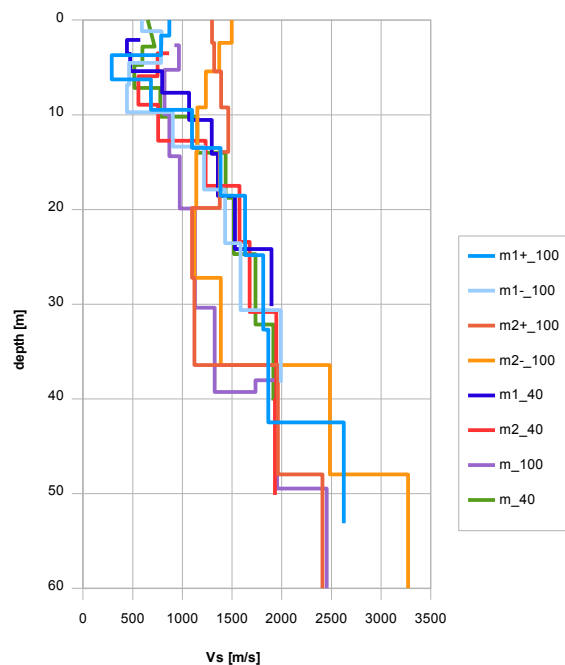Fig. 3.3j: Comparison of the ensemble of inversion results of both lines 09SN_02AIGLE-M1 and -M2, either using the 40 m- and the 100 m-arrays.
blue lines: analyses of records of line 09SN_02AIGLE-M1
red lines: analyses of records of line 09SN_02AIGLE-M2
violet line: mean of both 100 m-array records analyses in MINUS and PLUS direction.
green line: mean of all 40 m-array records analyses in MINUS and PLUS direction

3.3.7 Calculation of the shear wave velocity scalars $v_{s,5}$, $v_{s,10}$, …

The parameters $v_{s,5}$, $v_{s,10}$, $v_{s,20}$, $v_{s,30}$, $v_{s,40}$, $v_{s,50}$ represent the average shear wave velocities in the depth interval between the surface and the respective depth levels and are determined from the formula

$$v_{s,n} = \frac{\sum\limits_{i=1}^{n} d_i}{\sum\limits_{i=1}^{n} d_i/v_{si}} \quad \text{with:}$$

d_i = thickness of layer i
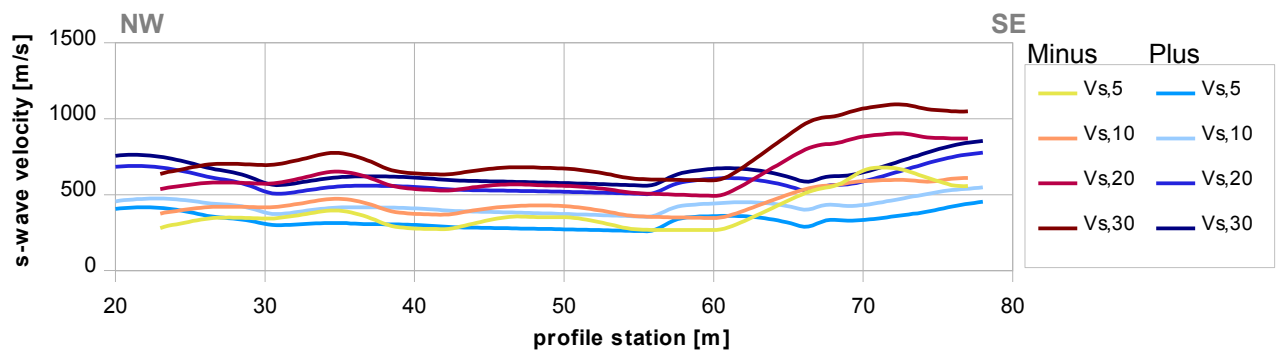v_{si} = corresponding shear-wave velocity.

Fig. 3.3k: *Graphs of the averaged $v_{s,5}$...-values along the line 09SN_02AIGLE-M1 for the PLUS- (blue lines) and MINUS- (red lines) directions.*
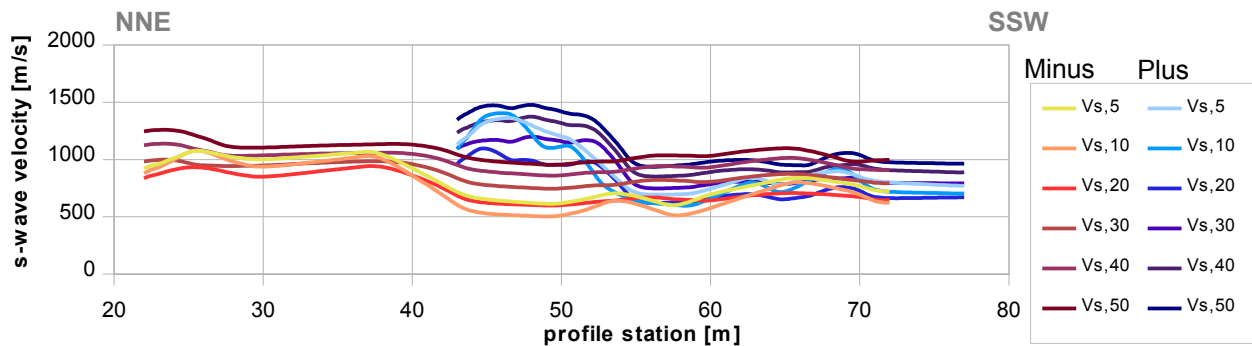

Fig. 3.3l: *Graphs of the averaged $v_{s,5}$...-values along the line 09SN_02AIGLE-M2 for the PLUS- (blue lines) and MINUS- (red lines) directions.*

The average values of the s-wave velocity model $v_{s,5}$, $v_{s,10}$, $v_{s,20}$, $v_{s,30}$, $v_{s,40}$, $v_{s,50}$, $v_{s,100}$ (= average shear wave velocity from the surface to depths of 5 m, …until 50 m) on the line segment nearest to the SED station (Tab. 3.3d) are summarized below:

	Vs,5	Vs,10	Vs,20	Vs,30	Vs,40	Vs,50
MINUS	594	574	855	1036	n/a	n/a
PLUS	349	456	620	684	n/a	n/a
MEAN	471	515	738	860	n/a	n/a

	Vs,5	Vs,10	Vs,20	Vs,30	Vs,40	Vs,50
MINUS	826	756	748	871	982	1069
PLUS	824	756	690	807	914	993
MEAN	825	756	719	839	948	1031

Tab. 3.3d: *The average shear wave velocities within the depth intervals from surface down to 5 m, etc.… to 50 m, calculated for the line segment with a subjectively most similar geology to the SED station (profile station 65 to 75 for line 09SN_02AIGLE-M1, above; profile stations 55 to 75 for line 09SN_02AIGLE-M2, below).*

3.4 Hybrid Seismic Data Processing

3.4.1 p-wave *Reflection* Seismic Processing Sequence

A) Data conditioning

A1 Reformatting and quality verification of field data
A2 Recording geometry assignment
A3 Data editing (suppression of bad / dead traces, etc.)
A4 Preliminary analysis of refraction velocities

B Filtering and deconvolution

B1 Analytical muting of refraction arrivals
B2 Amplitude recovery / amplitude equalization in time and frequency domains
B3 Predictive deconvolution parameter tests / application
B4 Determination of band limiting corner frequencies / application
B5 Optional 2-D filtering

C) Velocity analysis and stack

C1 Common Depth Point (CDP) sort
C2 Semblance velocity analysis using supergathers of 3 - 5 CDP's
C3 Optional dip move-out correction
C4 Normal Move-Out (NMO) correction and application of stretch mute
C5 Band-pass filtering
C6 CDP stack
C7 Optional coherency filtering

D) Time-depth conversion

D1 Optional spiking deconvolution
D2 Band-pass filtering
D3 Depth conversion
D4 Final display of seismic depth section with inversed polarity (non-SEG-convention)
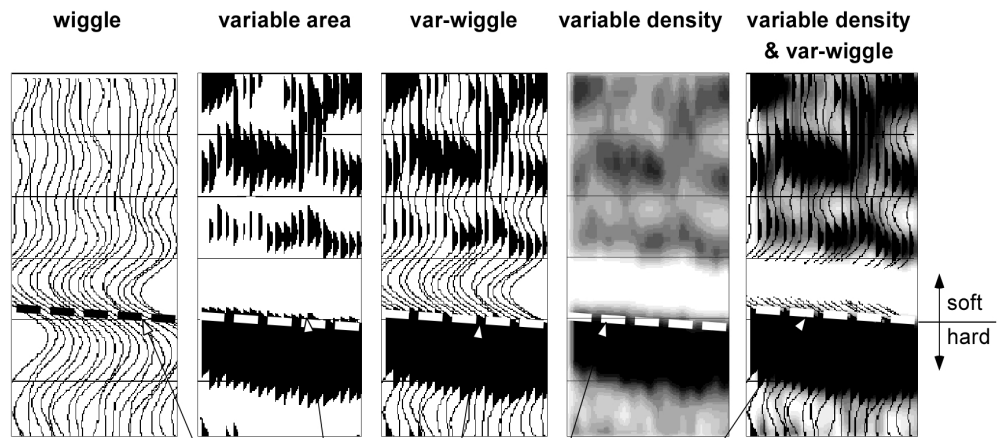
3.4.2 The presentation of reflection seismic data

The data in a reflection seismic section are presented as an assembly of individual seismic signals at regular intervals along a seismic profile. The simplest way of representing the signals are single wiggle lines (first to the left in the illustration below). A more capturing presentation is the variable area form (second to the left). Combining these two modes results in the var-wiggle mode. Another method of data visualization is the variable density mode (second from the right).

The compressional phase of seismic signals is defined in this report as the onset of the positive amplitude excursion in black (Fig. 3.4a). Since the source signal is produced by an explosion or by an impact at the surface, the signal starts off with a compression of the ground particles. Thus the arrivals of reflection events are defined by the compressional phase.

In rare situations of velocity inversions, cases in which formation velocities are lower than in the layers above, polarity reversals of the reflected signals occur. The beginning of the reflection event would then be characterized by a dilatational phase, represented in this report as a negative amplitude excursion, i.e. in white.

The final p-wave seismic depth sections are displayed in Fig. 3.4b and 3.4c, the hybrid sections in Fig. 3.4j and -k further below.

wiggle	variable area	var-wiggle	variable density	variable density & var-wiggle

soft
hard

Begin of the compressional phase defined at the time of the zero crossing of the positive amplitude excursion

Fig. 3.4a   Representation of reflection seismic data and the definition of a reflection event.
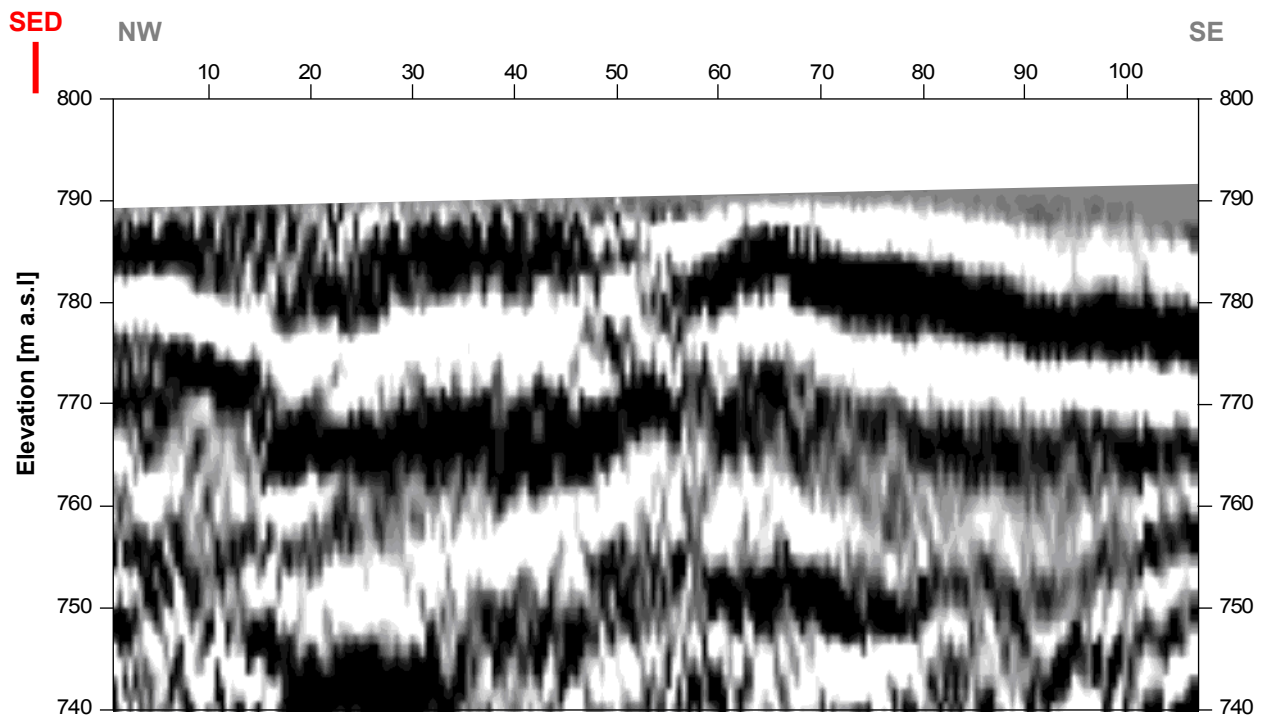
Fig. 3.4b: Seismic depth section of seismic line 09SN_02AIGLE-P1 with variable density mode present-
ation. Vertical axis: elevation [m a.s.l.], horizontal axis: profile meter; no vertical exaggeration.
The station spacing is 1 m.

Fig. 3.4c: *Seismic depth section of seismic line 09SN_02AIGLE-P2 with variable density mode present-ation. Vertical axis: elevation [m a.s.l.], horizontal axis: profile meter; no vertical exaggeration. The station spacing is 1 m.*
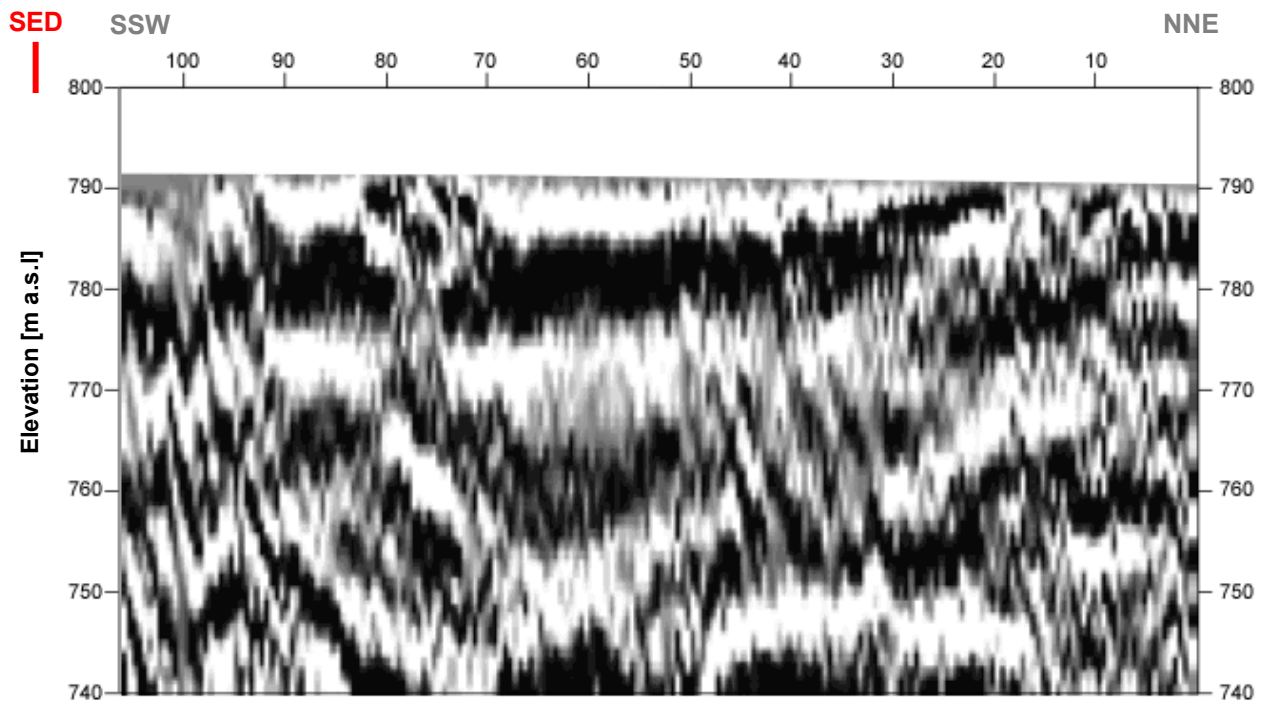
3.4.3   p-wave refraction tomography processing

The seismic p-wave refraction processing steps are analogous to those described in paragraph 3.2. For a detailed method statement and a description of the processing steps please refer to the summary report. The Figs. 3.4d to 3.4i and Tab. 3.4a illustrate the interme-diate processing steps and the final result.
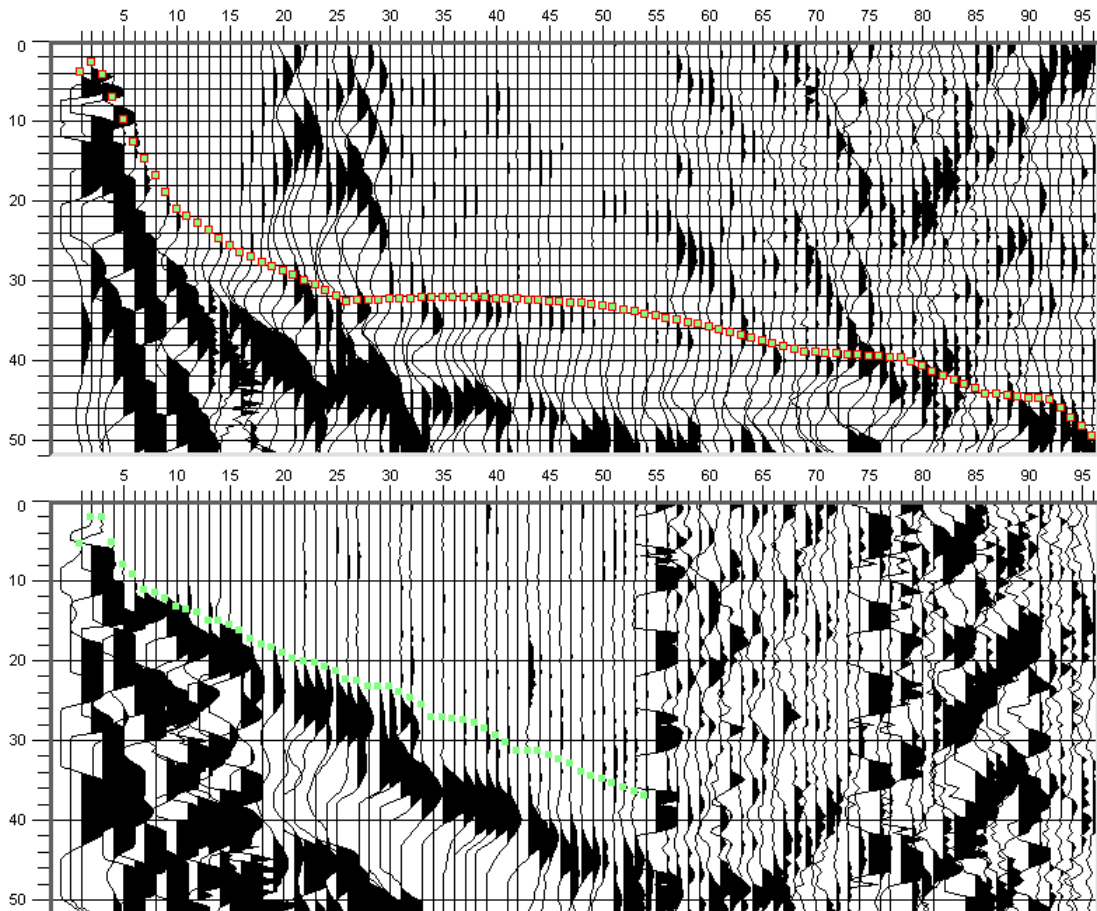

Fig. 3.4d: p-wave records of 09SN_02AIGLE-P1 (above) and -P2 (below) with positive amplitude excur-sions in black. Colored dots mark the manually picked first break arrival times. Vertical axis: travel time in ms, horizontal axis: station numbers spaced at 1 m.
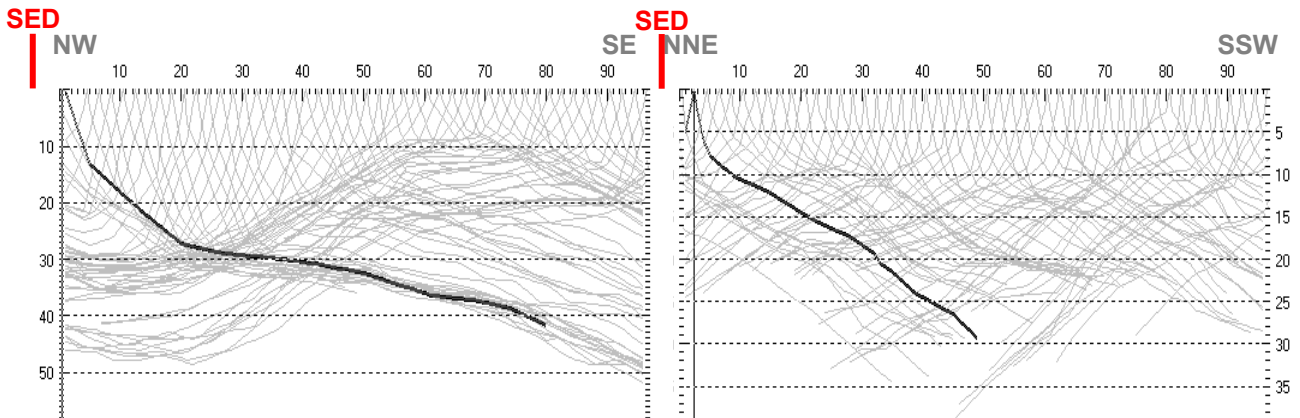
Fig. 3.4e: *Travel time curves of p-wave arrival time picks of line 09SN_02AIGLE-P1 (left) and -P2 (right). Vertical axes: travel time [ms], horizontal axes: station number (= profile meter).*
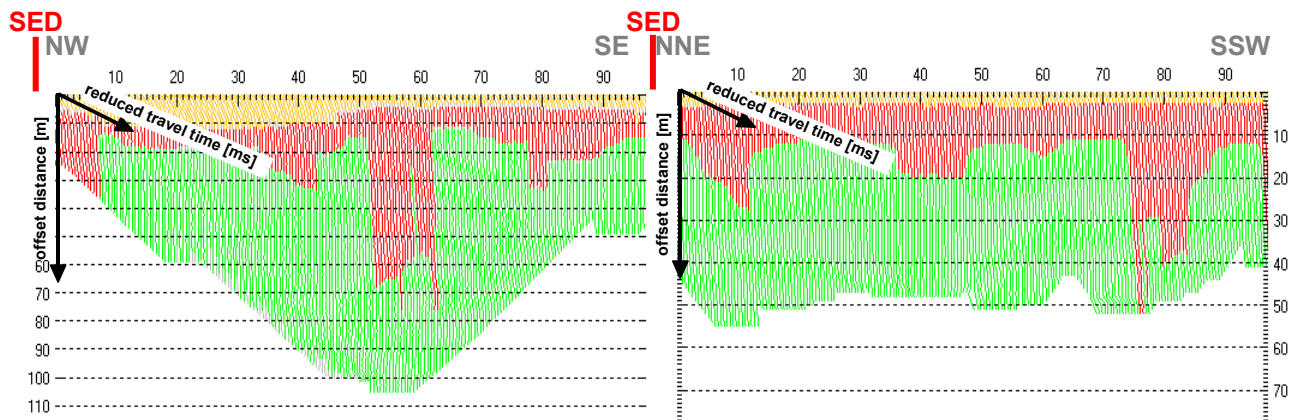

Fig. 3.4f: *3-dimensional distance-travel time diagrams at the mid-points between source points and re-ceiver stations are instrumental when using the analytical CMP derivation of the initial velo-city field. The horizontal axes are along the CMP positions and the travel time respectively, the vertical axis denotes the offset distance between source and receiver positions.*

Depth [m]	Vp [m/s]	Depth [m]	Vp [m/s]
0.0	173	0.0	164
0.2	298	0.2	332
0.5	351	0.5	401
1.2	515	0.7	515
1.7	680	1.2	850
2.4	944	1.7	1175
3.2	1373	2.4	1639
4.4	1909	3.2	2127
5.9	2423	4.2	2365
7.9	2715	5.6	2361
10.5	2887	7.3	2346
13.9	3231	9.5	2527
18.3	3813	12.4	1853
23.8	3532	16.1	2019
31.3	3913	20.8	2551
40.9	5530	26.8	3559
		34.6	4320

Tab. 3.4a: *Initial 1D p-wave velocity model derived from real data (left: 09SN_02AIGLE-P1; right: -P2).*
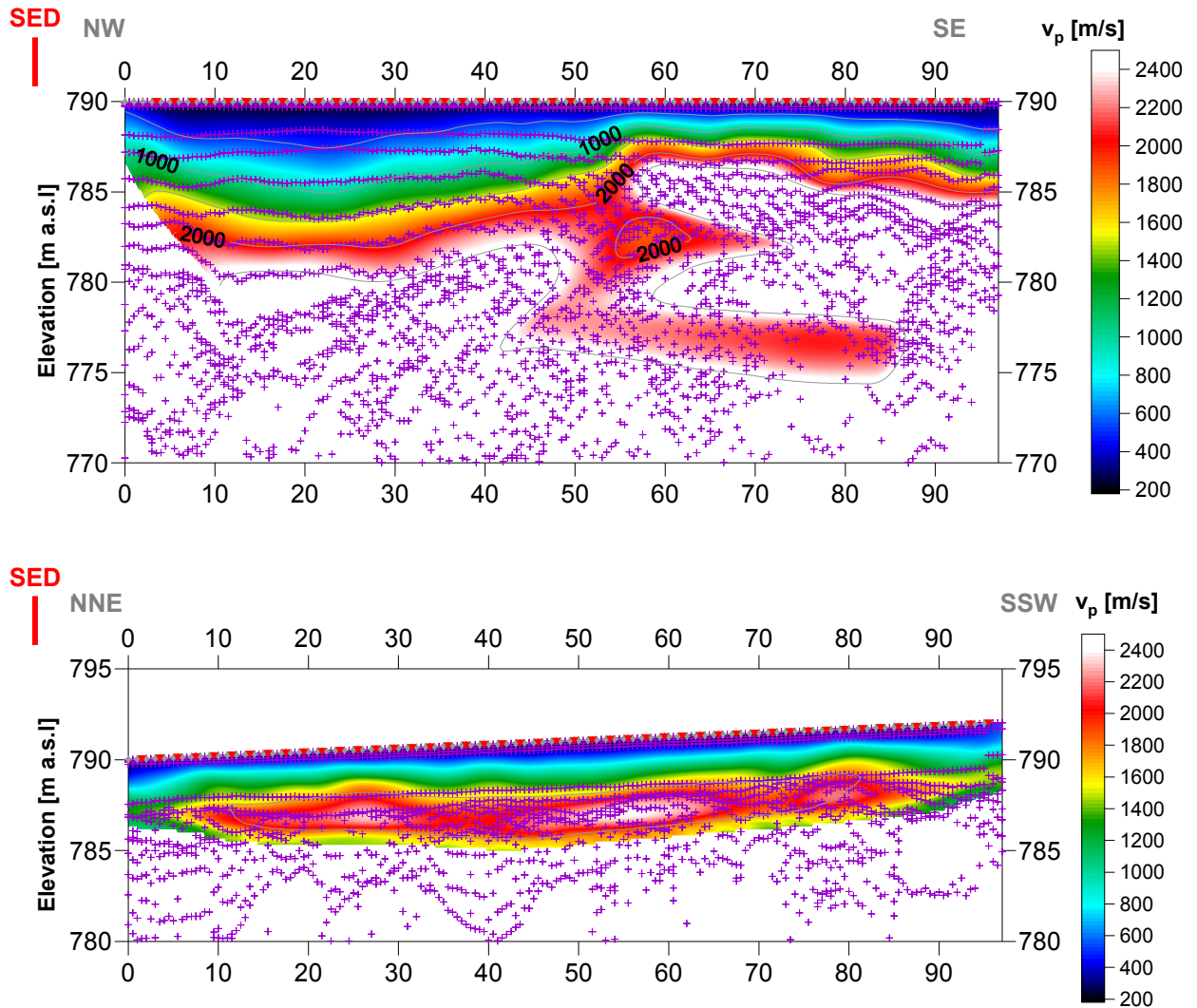
Fig. 3.4g: *Compressional wave velocity field image along the seismic profiles 09SN-02AIGLE-P1 (above) and -P2 (below). Red/white colors indicate solid rock, blue/black colors unconsolidated sediments and soil. Vertical axis: elevation [m a.s.l]; horizontal axis: profile meter; color scale: v_s [m/s]; vertical exaggeration: 2:1; gray squares: receiver stations; red triangles: shot positions; magenta crosses: positions of determined velocity values.*
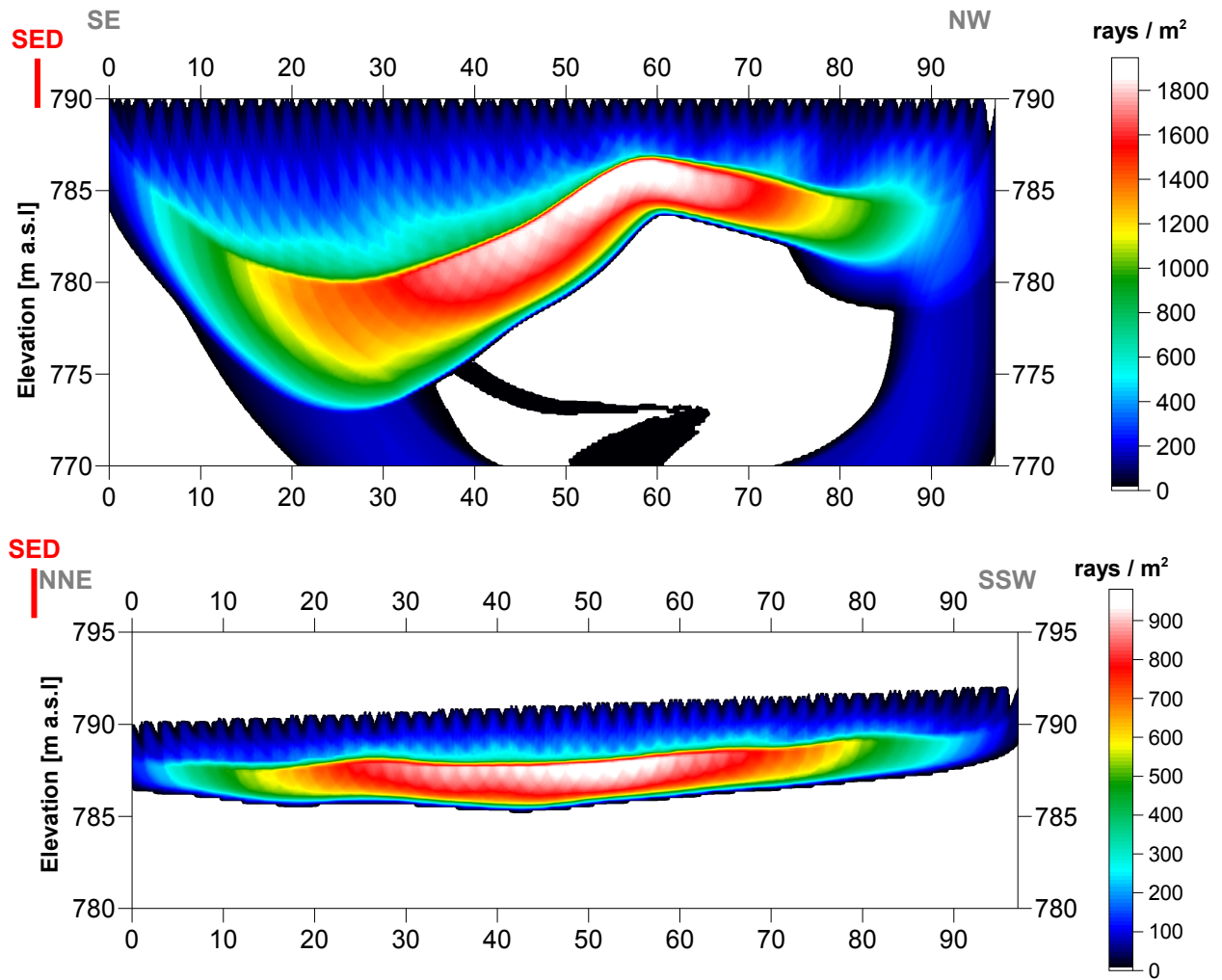
Fig. 3.4h   Compressional wave subsurface ray path density along the seismic profiles 09SN_02AIGLE-P1 (above) and -P2 (below). Red/white colors indicate high velocity contrast between two layers, blue/black colors low coverage areas. Vertical axis: elevation [m a.s.l]; horizontal axis: profile meter; color scale: ray paths per m2; vertical exaggeration: 2:1.

Depth [m]	Vp [m/s]
0.0	230
1.5	734
2.9	1220
4.2	1720
5.6	1980
6.9	2112
8.3	2286
9.6	2469
11.0	2509
12.3	2352
13.7	2432
15.0	2773
16.4	3049
17.6	3119
18.9	3060
20.3	2942
21.6	3080
23.0	3445

Depth [m]	Vp [m/s]
0.0	267
0.3	321
0.7	455
1.0	629
1.4	823
1.7	1023
2.0	1232
2.4	1486
2.7	1799
3.0	2064
3.4	2231

Tab. 3.4b: Final 1D p-wave velocity model derived from real data at positions most similar to the geological setting at SED station between profile meters 65 and 75 at line 09SN_02AIGLE-P1 (left) resp. 55 and 75 at line 09SN_02AIGLE-P2 (right) .
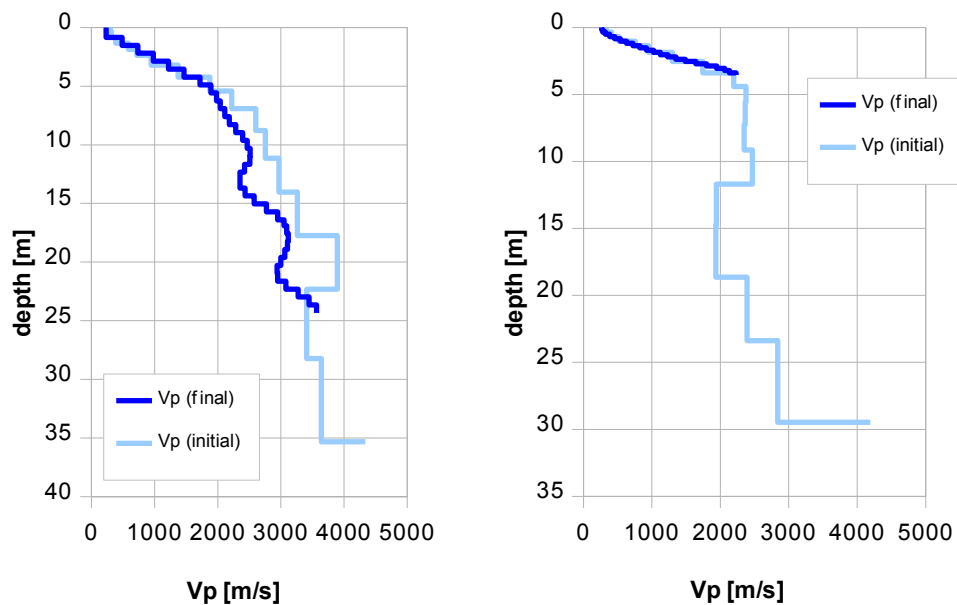
Fig. 3.4i: Final 1D p-wave velocity model derived from real data at a position most similar to the geological setting at the SED station between profile meters 65 and 75 at line 09SN_02AIGLE-P1 (left) resp. 55 and 75 at line 09SN_02AIGLE-P2 (right). Initial 1D p-wave velocity model values are given in Tab. 3.4a.

The relatively low depth of reached velocity information in profile 09SN_02AIGLE-P2 depends on methodological constraints: A high velocity contrast followed by a section of constant velocities can precisely detected by refraction tomography, but the underlaying section remains unvisible.

3.4.4 Representation of the hybrid seismic section

The hybrid seismic section is the reflection seismic section with the superimposed p-wave velocity field. It portrays the geological structures and the p-wave velocity field, the latter being indicative for the rock / soil rigidity. The uninterpreted hybrid seismic section is portrayed in Fig. 3.4j and 3.4k below.

Fig. 3.4j   Uninterpreted hybrid seismic section 09SN_02AIGLE-P1: superimposed onto the seismic reflection section is the color encoded p-velocity field derived by refraction tomography (no vertical exaggeration).
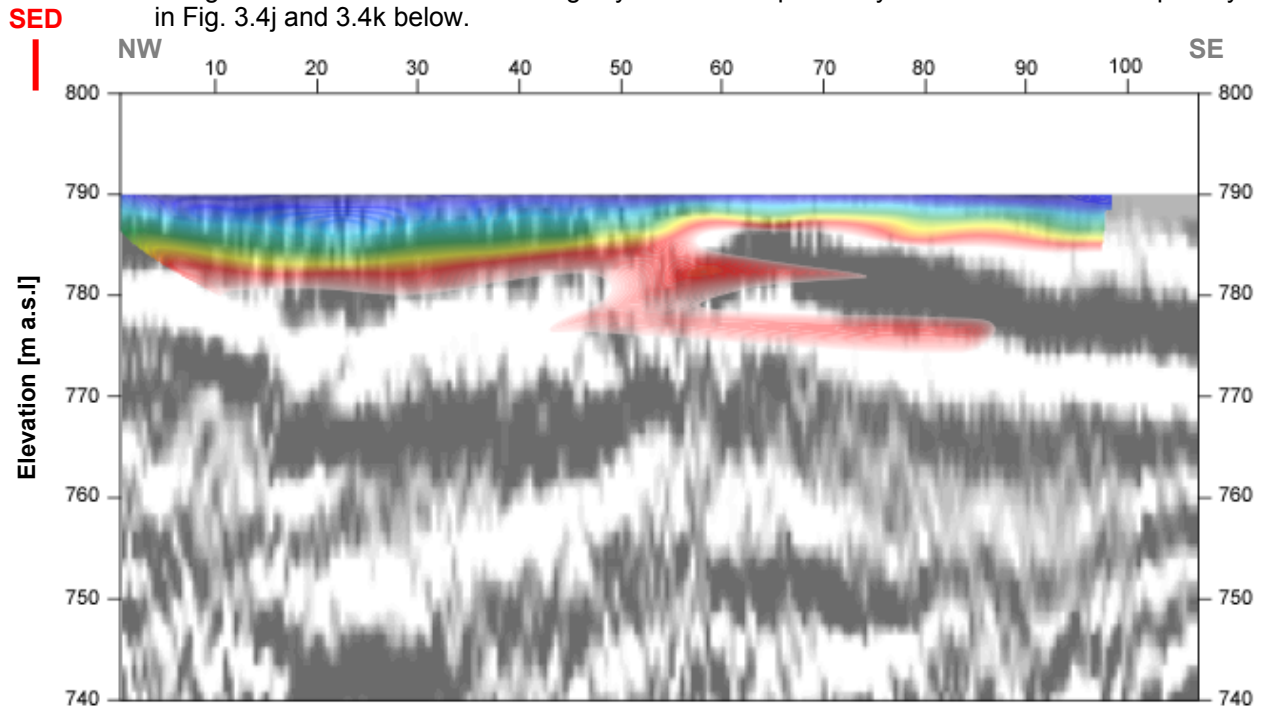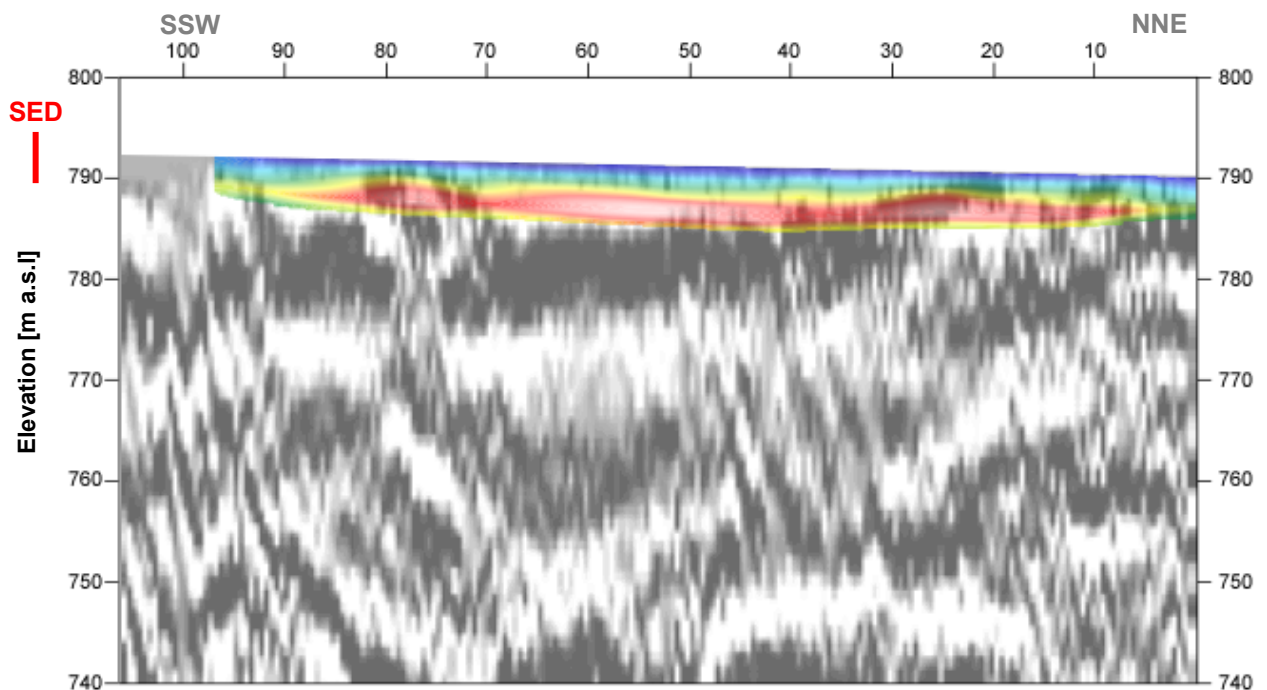

Fig. 3.4k   Uninterpreted hybrid seismic section 09SN_02AIGLE-P2: superimposed onto the seismic reflection section is the color encoded p-velocity field derived by refraction tomography (no vertical exaggeration).

4 DISCUSSION OF THE RESULTS

4.1 Summary and Validation of the Results

Compressional and shear wave velocity data from refraction seismic surveys both p-wave and s-wave and also the MASW survey data of profiles 09SN_02AIGLE-1 and 09SN_02AIGLE-2 are shown in Tab. 4.1 for the uppermost 30 m. The calculated shear wave velocity $v_{s(calc)}$ in Tab. 4.1 is derived by using a theoretical v_p/v_s-ratio of $\sqrt{3}$.

Depth	Vp1 meas	Vp2 meas	Vs1 meas	Vs2 calc	Vs1 meas	Vs2 calc	Vs1 MASW	Vs2 MASW
0	230	267		133	472	154		
1	485	539	485	280	516	311	466	837
2	734	1125	786	424	604	650	577	
3	1220	1946	1300	704	746	1124		866
4	1465	2231	1616	846	805	1288	443	
5	1891		1763	1092	982		476	
6	1980		2199	1143	1109			752
7	2112		2434	1219	1241			
8	2185		2318	1261	1387		798	
9	2286		2093	1320	1493			557
10	2469		1931	1425	1628			
11	2513		1809	1451	1642		1067	
12	2424		1752	1399	1599			
13	2352		1731	1358	1596			756
14	2432		1749	1404	1628		1295	
15	2577		1769	1488	1689			
16	2951		1779	1704	1717			
17	3093		1787	1786	1765			1233
18	3119			1801	1788			
19	3060		1804	1767	1827		1358	
20	2998		1827	1731	1846			
21	2942		1875	1698	1880			
22	3080		1931	1778	1898			
23	3275		1998	1891	1950			1575
24	3565		2068	2058	1986		1530	
25			2136		2023			
26			2200		2094			
27			2258		2134			
28			2311		2225			
29			2362		2268			
30			2412		2302		1899	
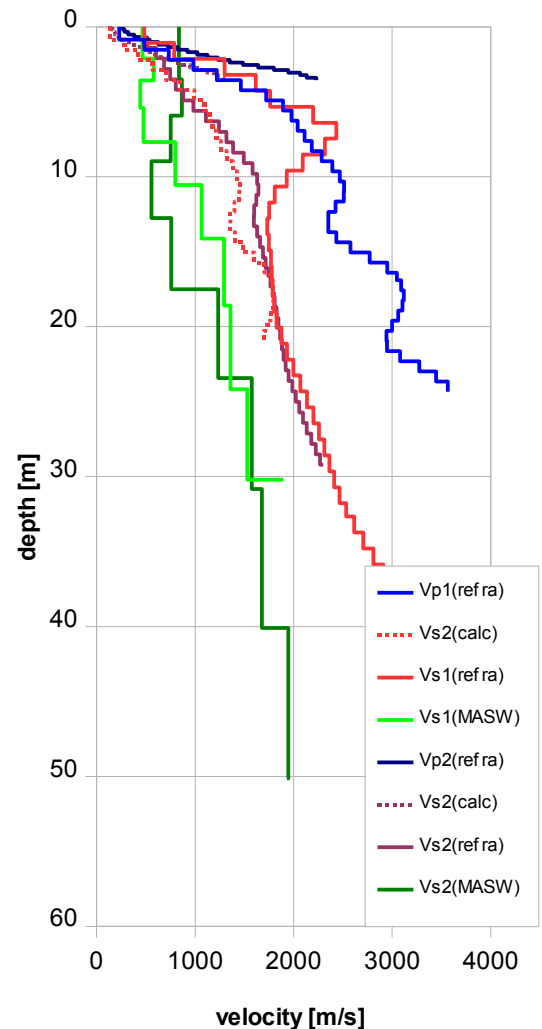
Tab. 4.1: Shear and compressional wave velocity model determined at the SED station AIGLE.

Fig. 4.1: Graphic display of shear (red lines) and compressional (blue lines) wave velocities determined at the SED station. In green colors values of MASW analyses. The results of line 09SN_02AIGLE-1 are given in lighter, and of line 09SN_02AIGLE-2 in darker colors.

4.2 Validation of the methods and their results

Due to methodological differences, v_s velocities derived by MASW analysis and by the refraction tomography technique may differ considerably. This is because MASW analysis cannot image small rock/soil inhomogeneities as a dispersion image with an array length of i.e. 40-m only yields one single v_s-value at each depth. On the other hand, refraction diving wave tomography results produce v_s-sections with a high lateral resolution, but fail to provide information at greater depths.

4.3   Error Estimates

The error estimates given in Tab. 4.3 below are relevant only in the context of this survey.

Surveying method	Type of result	Error estimate
v_s – refraction tomography	v_s – velocity field image	10%*
MASW only "+" or only "-" values	v_s – velocity field image	30%
MASW (mean of "+" & "-" values)	v_s – velocity field image	20%
v_p – refraction tomography	v_p – velocity field image	10%
Reflection seismic surveying	Image of subsurface structures	n.a.

* v_s at line 09SN_02AIGLE-S2 potentially contents too high velocities, in 8 m depth. The results may base on p-s-converted waves. Above and below, the values fit the data derived from line 09SN_02AIGLE-S1 and the theoretical calculation from p-wave refraction values.

Tab. 4.3   Error estimates for the methods applied. Note that higher error estimates are to be taken into account with increasing depths.

At the SED station AIGLE (Corbeyrier VD), the refraction velocity images both from shear and compressional wave analysis show coincident structures. The MASW figures are in the top 5 meters higher and in the bottom 25 m lower than in the shear wave refraction survey.

4.4   The Geophysical Interpretation

The most conclusive information about the subsurface structures is provided by the results of the hybrid seismic section (v_p-refraction tomography profiling and reflection seismic section) and confirmed by the evaluation results of the v_s-refraction tomography data.

As can be seen from the v_s and v_p refraction tomography sections in Fig. 3.2e/f & Fig. 3.4g/h, the topography of the bedrock surface is imaged in detail on both profiles. The geological interpretation of the seismic events is shown in Fig. 4.2a. The rock surface topography shows a depression to the Northwest (max. depth of 6 m) with a local ridge in the middle of the seismic profile. In Southeast, the unconsolidated cover has a thickness of maximal 4 m.

Just in the middle and also in the Northwest (20 m from the portal), tectonic faults are clearly visible. The middle one coincides with the SE-end of the dell in rock's topography.
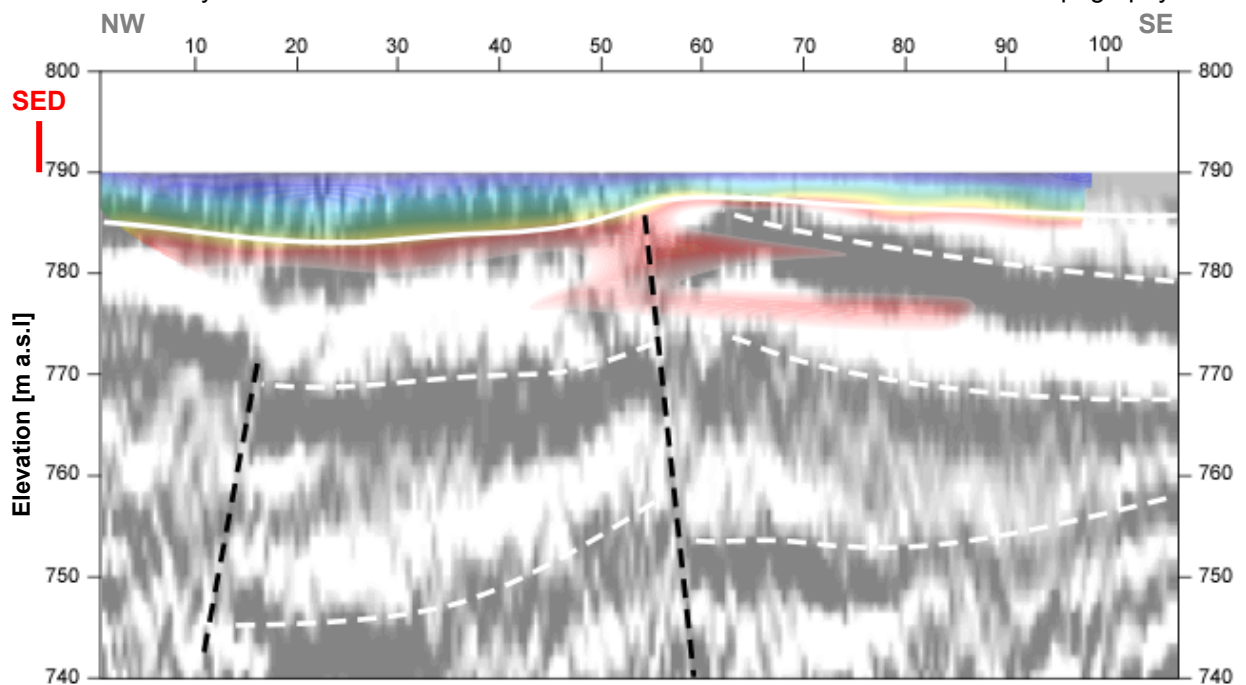

Fig. 4.2a   Geophysical interpretation of the hybrid seismic section 09SN_02AIGLE-P1. White lines denote layer boundaries, continuous line the bedrock surface. The black hatched lines follow the supposed tectonic faults.

The geological interpretation of the seismic events of line 09SN_02AIGLE-2 is shown in Fig. 4.2b. The consolidated rock topography seems to be in less than 3 m depth all over the seismic section. No clearly visible layering in the rock is imaged.

Two tectonic faults are vaguely indicated outcropping at stations 80, resp. 40.
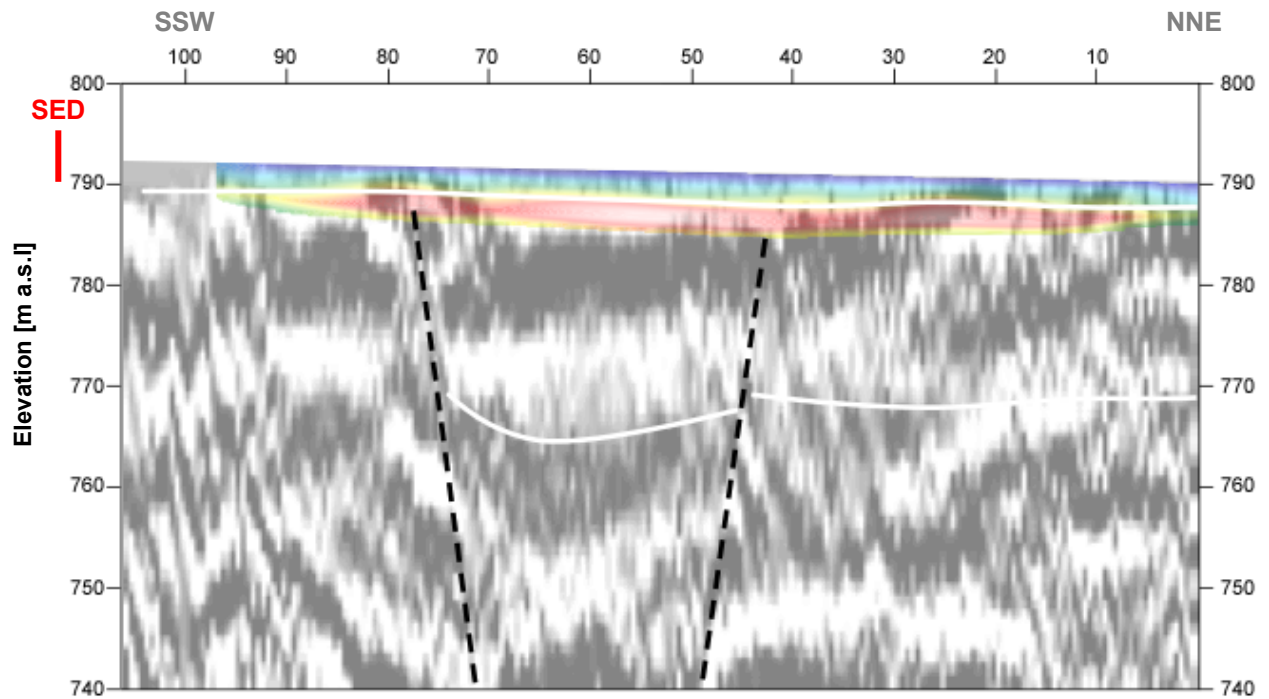

Fig. 4.2b *Geophysical interpretation of the hybrid seismic section 09SN_02AIGLE-P2. White lines denote layer boundaries, the continuous one marks the bedrock surface; black dotted lines are indicative of suspected faulting.*

5 SUMMARY AND CONCLUSIONS

◆ In April 2009 a combined seismic s- and p-wave survey was carried out at the SED earthquake monitoring station AIGLE (Corbeyrier VD).

◆ The shear wave data have been evaluated by conventional diving wave refraction tomography techniques in order to derive the s-wave velocity field along the seismic line.

◆ The p-wave data have been processed

  • firstly to derive a 2D s-wave velocity field by using the MASW (**M**ultichannel **A**nalysis of **S**urface **W**aves) technique;

  • and secondly, according to the hybrid seismic data processing scheme for representing the subsurface structures in a combined reflection seismic section with the superimposed p-wave velocity field.

◆ The shear wave velocity range determined by the MASW method in the uppermost 30 meters spans from values of 443 m/s to 1899 m/s.

◆ The scalar values derived by the MASW survey at the SED station (seismic line 09SN_02AIGLE-M1, profile station 70; seismic line 09SN_02AIGLE-M2, profile station 65) are the following:

line 1			line 2		
$v_{s,5}$	=	471 m/s	$v_{s,5}$	=	825 m/s
$v_{s,10}$	=	515 m/s	$v_{s,10}$	=	756 m/s
$v_{s,20}$	=	738 m/s	$v_{s,20}$	=	719 m/s
$v_{s,30}$	=	860 m/s	$v_{s,30}$	=	839 m/s
$v_{s,40}$	=	n/a	$v_{s,40}$	=	948 m/s
$v_{s,50}$	=	n/a	$v_{s,40}$	=	1031 m/s

◆ The accurate refraction shear wave velocity for consolidated rocks is 1820 m/s, found at a depth of 20 m.

◆ The maximum p-wave velocity determined is 3565 m/s at a depth of 24 m.

◆ The geophysical interpretation of the subsurface structures in this report are to be validated and incorporated into a comprehensive appraisal by a geologist familiar with the local geological setting.

Schwerzenbach, 12th June 2009

Walter Frei
dipl. Natw. ETH
managing director

Lorenz Keller
dipl. Natw. ETH
project manager